

In-vitro cell line studies



5. IN-VITRO CELL LINE STUDIES

5.1 Introduction

After the preliminary studies at formulation preparation and characterization, the final objective was to deliver these nanoparticulate carriers by parenteral route to animals. But before the animal studies, the formulations should be evaluated for their safety and efficacy at tissue culture level. The aim of the study was to evaluate prepared NPs for cancer chemotherapy with a view to explore the possible effects of particle size, conjugation and particle surface coating on the cell uptake. Hence, the cell uptake, phagocytosis, cell cycle analysis, apoptosis and cytotoxicity studies were taken up prior to in-vivo studies. Cell uptake studies were carried out using 6-coumarin (lipophilic fluorescent dye) loaded NPs with the aim of finding whether the NPs are internalized into the cells and to determine the intracellular concentrations of the loaded dye. The inhibition of FPP synthase by ZOL causes accumulation of isopentenyl pyrophosphate (IPP), which further converted to ApppI were estimated using LC-ESI-MS in MCF and BO2 cell lines.

5.2 Materials

DMEM 21885, DMEM 31885, FBS, PBS, Penicillin, streptomycin, trypsin, EDTA, HBSS were purchased from GIBCO, Finland. RPMI 1640 was purchased from Lonza, Finland. 3-(4,5-Dimethylthiazol-2-yl)-2,5-diphenyltetrazolium bromide (MTT) and Propidium Iodide (PI) were purchased from Sigma Chemicals, Finland. All well plates and tissue culture flask were purchased from NUNC, Finland. Hoechst 33342 and RNase A was purchased from Invitrogen, Finland. Annexin V-FITC and binding buffer were purchased from Biolegend. 6-coumarin was purchased from Sigma Aldrich, India. HCl, NaOH, SDS, DMF and DMSO were obtained from S. D. Fine Chemicals, India. Lysotracker red dye was purchase from Invitrogen (Finland). Water used for LC-ESI-MS was purified in a MilliQ Gradient purification system (Millipore, Bedford, MA, USA) and HPLC-grade methanol (MeOH) was purchased from Labscan Ltd. (Dublin, Ireland). N,N-dimethylhexylamine (DMHA) was from Aldrich (Milwaukee, WI, USA), methyleneadenosine 5'-triphosphate (AppCp), bovine serum albumin and sodium orthovanadate (Na_3VO_4) were from Sigma Chemical Co. (St. Louis, MO, USA) and sodium fluoride (NaF) from Riedel-de-Haen (Seelze, Germany). Triphosphoric acid 1-adenosin-5'-yl ester 3-(3-methylbut-3-enyl) ester

(AppI) was synthesized at the Department of Chemistry at University of Eastern Finland.

5.3 Cell culture

RAW 264 cell line is a mouse macrophage cell line, obtained from The American Type Culture Collection (ATCC) (USA) and maintained in DMEM 21885 GLUTMAX® media supplemented with 10% FBS. MCF7 cell line is a human breast cancer cell line, obtained from European Collection of Cell Cultures (ECACC) (Salisbury, UK) and maintained in RPMI 1640 Biowhittaker® media supplemented with 10% FBS. BO2 cell line obtained from INSERM, Research Unit 664, IFR62, Faculte de Medicine Laennec, Lyon, France and maintained in DMEM 31885 GLUTMAX® media along with 10% FBS. BO2, a subclone of MDA-MB-231, has been derived after six in vivo passages in nude mice and characterized by its unique morphology and affinity resembling to bone metastasis (Peyruchaud et al, 2001). All Cell lines were cultured at 37°C in a 5% CO₂ and 90 % RH humidify atmosphere and handled in sterile condition.

5.4 Opsonization and phagocytosis

Opsonization is the process by which a foreign organism or particle becomes covered with opsonin proteins, thereby making it more visible to phagocytic cells. After opsonization, phagocytosis can occur, which is the engulfing and eventual destruction or removal of foreign materials from the bloodstream. Together these two processes form the main clearance mechanism for the removal of undesirable components larger than the renal threshold limit from the blood. In the case of polymeric nanoparticles, which cannot normally be destroyed by the phagocytes, sequestration in the MPS organs typically occurs. If the polymeric nanoparticle is non-biodegradable, then accumulation of particles in these organs, most commonly the liver and spleen, can occur leading to toxicity and other negative side effects (Illum et al., 1986; Peracchia et al., 1999a).

The macrophages of the MPS have the ability to remove unprotected nanoparticles from the bloodstream within seconds of intravenous administration, rendering them ineffective as site-specific drug delivery devices (Gref et al., 1994). The preferred method of imparting stealth, or sterically stabilized properties to nanoparticles is

through the PEGylation of these particles. PEGylation simply refers to the decoration of a particle surface by the covalently grafting, entrapping, or adsorbing of PEG chains. The purpose of these PEG chains is to create a barrier layer to block the adhesion of opsonins present in the blood serum, so that the particles can remain camouflaged or invisible to phagocytic cells. (Peracchia et al., 1999b).

Macrophage lineage of liver and spleen are associated with opsonization and subsequent removal of harmful foreign body from blood. This condition can be simulated *in vitro* using RAW 264 cell line which is basically macrophage cell line, demonstrate opsonization and/or compliment consumption characteristic as well. This tool was selected for estimation purpose of antiopsonization liability of NP and quantitative comparison among different NPs uptake with time. All PLGA NPs were prepared with entrapped fluorescence dye 6-coumarin as a marker to estimate amount of NPs by cells using very specific and selective fluorescence assisted cell sorting (FACS) technique. Uptakes of NPs were also confirmed by microscopy using confocal microscope (Carl Zeiss, Axiovert 135M) which demonstrated similar observations which supported our findings using FACS technique.

5.4.1 Cell line protocol for phagocytosis (macrophage uptake)

RAW264 cells were seeded in 6 well plates at the density of 1×10^5 cells per well and incubated for 48 h to allow cell attachment. After 48 h, cells were treated with 100 $\mu\text{g/ml}$, 2 ml of 6-coumarin loaded PLGA NPs and different PEGylated PLGA NPs followed by incubated for 60, 120 and 240 min for phagocytosis. PLGA-PEG NPs with different PEG content (10%, 20% and 30%) were used in the study. After treatment all well plate were washed with cold HBSS buffer twice and each well was treated with Sodium Azide (10 mM) to prevent NP flux. The cells were harvested by treatment with trypsin-EDTA followed by centrifugation and resuspended in PBS. Samples were kept at 4°C with light protection and FACS analysis was performed within 1 h. In FACS analysis, 10,000 cells were counted and analysed by measuring signal from FITC channel (Canto-II, BD). Experiment was performed in triplicates.

5.4.2 Macrophage uptake of PLGA NP

For further *in vitro* antiopsonization evaluation, cell uptake study was performed with mouse macrophage cell line RAW264. Results shows that in all formulations, PLGA-

PEG30 NP and PLGA-PEG20 NP showed least phagocytic uptake in all time points which is five times less in compare to PLGA NP. Although, PLGA-PEG30 NP shows no added advantage of increase in PEG grafting over PLGA-PEG20 NP. As the time progressed, phagocytic uptake of all NP formulations was very slightly increased. PLGA-PEG10 displayed marginal resistance to phagocytosis as cellular uptake is reduced by 1/5 at all time point in compare to PLGA NPs. PLGA NPs followed by PLGA-PEG10 showed high phagocytic uptake among all formulations showing its high vulnerability to opsonization (Table 5.1; figure 5.1).

Table 5.1: Phagocytic uptake of 6-coumarin loaded PEGylated PLGA NP formulations by mouse macrophage cell line RAW264 after incubation for 60, 120 and 240 min using FACS as estimation technique. Data presented as Mean \pm SEM, n = 3.

Sr. No.	Formulation	Time (min)	% Microphage uptake			Mean of % uptake
1.	PLGA NP	60	51.41	48.31	43.94	47.88
		120	52.42	52.53	42.02	48.99
		240	55.72	55.92	42.86	51.50
2.	PLGA-PEG10 NP	60	41.69	40.70	30.54	37.64
		120	42.05	43.73	30.98	38.92
		240	44.59	34.51	30.34	36.48
3.	PLGA-PEG20 NP	60	8.35	9.45	10.10	9.30
		120	12.34	12.93	11.49	12.26
		240	12.06	14.12	12.00	12.73
4.	PLGA-PEG30 NP	60	9.05	8.64	10.64	9.44
		120	12.41	10.71	12.71	11.94
		240	13.74	14.19	13.05	13.66

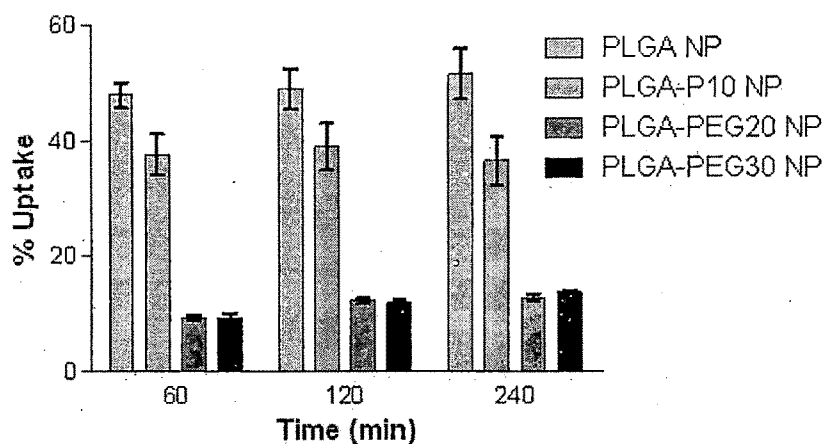


Figure 5.1: Phagocytic uptake of 6-coumarin loaded PEGylated PLGA NP formulations by mouse macrophage cell line RAW264 after incubation for 60, 120 and 240 min using FACS as estimation technique. Data presented as Mean \pm SEM, n = 3.

5.4.3 Microphage uptake of PBCA NP

PBCA-PEG20 NP showed tremendous protein repellent property under *in vitro* condition which indicates its ability to prolong circulation half life *in-vivo*. Further, to confirm *in vitro* antiopsonization activity, phagocytic study was performed with mouse macrophage cell line RAW264. Results showed, among the tested formulations, PBCA-PEG20 showed least phagocytic uptake and the decrease is about seven times less in comparison to PBCA NP. PBCA-PEG10 and PEG-PBCA-PEG also displayed moderate resistance to phagocytosis as the cellular uptake is about three times less than PBCA NP. Comparing PBCA-PEG formulations containing varied concentration of PEG (5%, 10% and 20%), phagocytic uptake decreased drastically with increase in PEG concentration from 5% to 10% while further increase to 20% showed a moderate influence (Fig. 2; Table 2) which may probably due to saturation in the phagocytic inhibition process. Phagocytosis increases modestly with time in all formulations. At 240 min time point all histogram showed split distribution showing signs of NP degradation in macrophage as florescence intensity start diminishing intracellularly after phagocytosis (Fig. 3). Phagocytic uptake was also observed under confocal microscope after incubation of 6-coumarin loaded PBCA NP

and PBCA-PEG20 NP with RAW 264 cell line. Cell nucleus was stained with Hoechst 33342. Results showed significant increase in cellular uptake of PBCA NP in comparison to PBCA-PEG20 NP (Fig. 4).

Table 5.2: Phagocytic uptake of 6-coumarin loaded PEGylated PBCA NP formulations by mouse macrophage cell line RAW264 after incubation for 60, 120 and 240 min using FACS as estimation technique. Data presented as Mean \pm SEM, n = 3.

Sr. No.	Formulation	Time (min)	% cell uptake			Mean of % cell uptake
1.	PBCA NP	60	52.01	46.83	43.76	47.53
		120	55.44	48.85	43.71	49.33
		240	60.10	55.86	45.11	53.69
2.	PBCA-PEG5 NP	60	37.41	36.04	34.10	35.85
		120	39.08	36.29	33.06	36.14
		240	47.01	39.64	32.17	39.61
3.	PBCA-PEG10 NP	60	13.81	12.84	12.47	13.04
		120	15.65	13.49	13.88	14.34
		240	15.58	12.55	12.53	13.55
4.	PBCA-PEG20 NP	60	7.96	6.87	5.82	6.88
		120	8.61	7.37	6.08	7.35
		240	8.84	8.27	6.39	7.84
5.	PBCA-PEG-PBCA NP	60	16.80	17.88	12.73	15.80
		120	18.30	19.71	13.10	17.04
		240	19.15	19.86	10.60	16.54

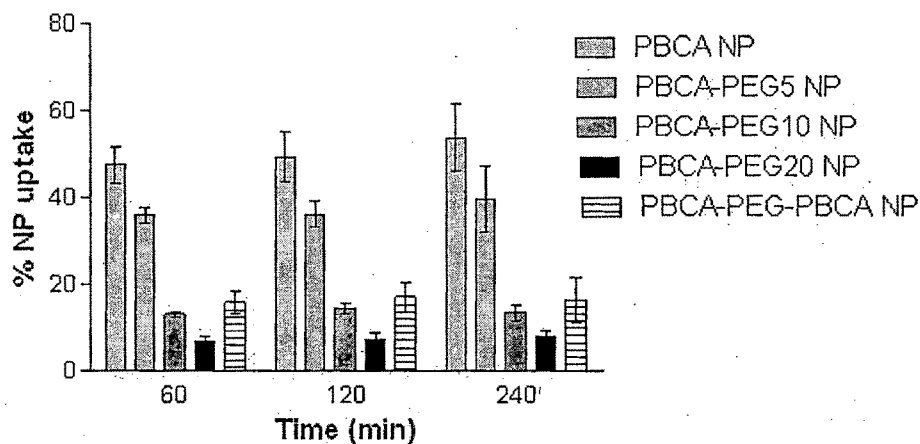


Figure 5.2: Phagocytic uptake of 6-coumarin loaded PEGylated PBCA NP formulations by mouse macrophage cell line RAW264 after incubation for 60, 120 and 240 min using FACS as estimation technique. Data presented as Mean \pm SEM, n = 3.

In this study, macrophage cell line RAW 264 was used which is mouse macrophage cell line and widely used for *in vitro* phagocytosis studies of NPs (Liu et al, 2009). We have evaluated comparative cellular uptake of NPs at three different time point to determine phagocytosis kinetics where it was found that phagocytosis increases in a time dependent manner. Up take was found to increase with time, but decreases with increase in PEG density. These results are in relevance with earlier reports (Mosqueira et al, 1999). However incase of PBCA-PEG-PBCA cellular uptake is high in comparison to PBCA-PEG20 which is having lesser PEG density. This observation demonstrates the effect of orientation of PEG in NP on cellular uptake. In case of PBCA-PEG20, PEG has possibly oriented tangentially making 'brush configuration' while in case of PBCA-PEG-PBCA, PEG has oriented in circular bended U shape making 'flower configuration'. It is well establish that steric repulsion effect to serum protein depends of 'dynamic hydrophilic cloud', chain length and chain flexibility (Gref et al, 1995; Gref et al, 2000). In both configurations, it can be inferred that 'brush configuration' displays clear advantage as more dynamic hydrophilic cloud volume, chain length and chain flexibility. In 'flower configuration' because of both ends of PEG in bound form which reduce size of hydrophilic cloud, chain length and also reduce chain flexibility in compare to brush configuration (Peracchia et al, 1997).

PBCA-PEG-PBCA has more PEG content still have less resistance to phagocytosis in comparison to PBCA-PEG20 NPs.

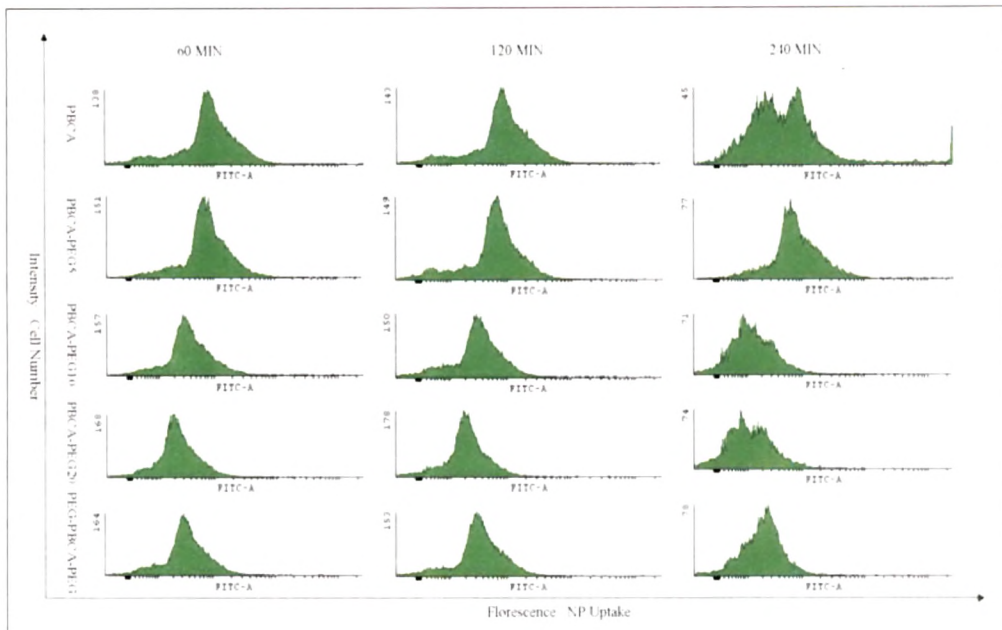


Figure 5.3: Phagocytic uptake histograms of 6-coumarin loaded NP formulations by mouse macrophage cell line RAW 264 after incubation for 60, 120 and 240 min using FACS as estimation technique.

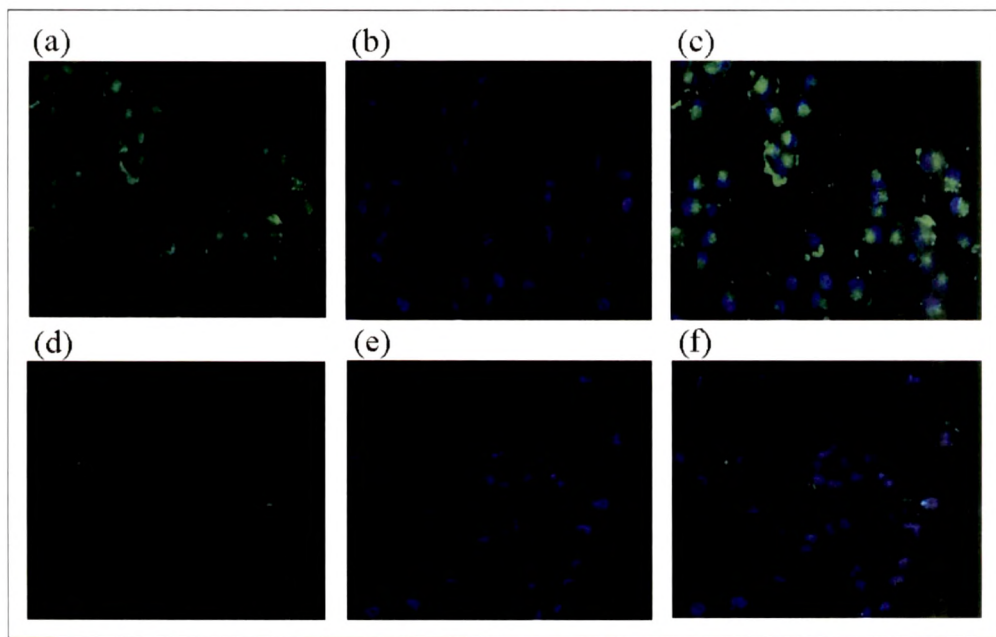


Figure 5.4: Microscopic evaluation of phagocytic up takes of PBCA NP and PBCA-PEG20 NP using confocal microscope. (a to c) show images for PBCA NP and (d to f) shows images for PBCA-PEG20 NP. (a) & (d) coumarin6 loaded NP uptake (b) & (e) nucleus stained using Hoechst 33342 and (c) & (f) overlapping images

5.5 Cell up take by MCF7 and BO2 cell line

The primary advantage in using macromolecules as drug delivery vehicles is their mechanism(s) of cellular internalization. The cell membrane is naturally impermeable to complexes larger than 1 kDa; however, cells possess a variety of active internalization mechanisms to accommodate cellular entry of large molecular complexes. Here, the cell membrane will invaginate to engulf molecules and extracellular fluid in an intracellular membrane bound vesicle, or endosome, that will subsequently traffic through the cell, a process known as endocytosis (Castino et al, 2003). Molecules may reside near the membrane or directly interact with membrane proteins to enable their retention in these vesicles. Analogous to the attachment of drug moieties to high molecular weight carriers, agents such as antibodies and high affinity ligands can be incorporated in order to exploit direct membrane interactions and target these complexes to specific cell populations in organ systems. Once inside the cell, the intracellular fate of the endosomal contents is an important determinant of successful drug delivery. Depending on the membrane interaction and components involved in vesicle formation, endosomes will mature into acidic vesicles which may or may not fuse with lysosomes, which can completely metabolize macromolecules using hydrolytic and enzymatic reactions. Targeting macromolecular complexes with high affinity ligands specific to membrane proteins, namely receptors, can aid in regulating not only the cellular recognition of these carriers but also the trafficking pathway and subcellular localization within the cell (Sly et al, 2002).

The major objectives for targeted drug delivery are reducing the nondiscriminate uptake of toxic agents as well as enhancing drug accumulation at the target site. In order to target drugs to specific tissue systems within the body, drug molecules can be directly attached to a targeting agent or complexed with a vehicle, or macromolecule, that contains targeting moieties. Macromolecules can be bioengineered to incorporate a variety of synthetic and natural compounds including drugs, ligands, and radionuclides (Bareford and Swaan; 2007).

5.5.1 Cell line protocol for cell uptake

Cells were seeded on 6 well plates at the density of 1×10^5 cells per well and allowed to attach and grow. After 48 h, cells were incubated with 1 ml, 100 $\mu\text{g/ml}$ 6-coumarin loaded PLGA-PEG20 NPs and PLGA-PEG-ZOL NPs for 30 and 90 min. Cells were washed, harvested and analysed in FACS (Canto-II, BD) for total amount of NP uptake by 10,000 cells. Same treatment as above was also performed in cell incubated micro-slide for purpose of microscopy. After adequate treatment adherent cells were washed and analyzed under confocal microscope (Carl Zeiss, Axiovert 135M). The cell uptake route characterization was performed for 6-coumarin loaded PLGA-PEG20 NPs and PLGA-PEG-ZOL NPs using various cell uptake route inhibitors as listed in table 1. After treatment with specific inhibitor, each well was tested for cell uptake of 6-coumarin loaded PLGA-PEG20 NPs and PLGA-PEG-ZOL NPs using FACS.

5.5.2 PLGA NP uptake by cancer cell

NP uptake was evaluated in MCF7 and BO2 cell line and result displayed in fig. 4a and fig. 4b respectively. In MCF7 cell line, uptake of PLGA-PEG-ZOL NPs was found 32.77% that is higher as compared to PLGA-PEG20 NP at 30 min time point. The increased uptake at 60 min and 120 min time points was found to be 34.08% and 37.4%, respectively (fig. 5.5; Table 5.3). In case of BO2 cell line internalization of PLGA-PEG-ZOL NPs was enhanced up to 36.51% in comparison to PLGA-PEG20 NP at 30 min time point. After 60 min and 120 min the increase in uptake is 27.16% and 30.32% in comparison to PLGA-PEG20 NP (Fig. 5.6; Table 5.3). The enhanced uptake is resulted because of activation of addition endocytosis pathway, caveolae mediated endocytosis, along with clathrin mediated endocytosis. Both are receptor mediated pathways which followed saturable kinetic. NP capable of endocytic uptake by more than one pathway reasonably increases the amount of NP uptake.

NP uptake by cancerous cell line usually occurs by endocytosis process. It can be speculated that the enhanced uptake is a consequence of better interaction of ZOL grafted NP with cell membrane resulting higher endocytosis uptake and/or higher residence time of ZOL grafted NP in intracellular domain.

Table 5.3: Endocytic uptake of 6-coumarin loaded PLGA-PEG20 NP and PLGA-PEG-ZOL NP in human breast cancer cell line (a) MCF7 and (b) BO2 after incubation for 30, 60 and 120 min using FACS as estimation technique. Data presented as Mean \pm SEM, n = 3.

Cell line	Formulation	Time (min)	% cell uptake			Mean of % cell uptake
MCF7	PLGA-PEG20 NP	30	42.91	47.09	45.09	45.03
		60	49.48	54.21	52.07	51.92
		120	61.41	63.93	62.47	62.60
	PLGA-PEG-ZOL NP	30	77.24	78.27	77.88	77.80
		60	85.11	87.65	85.24	86.00
		120	100.00	100.00	100.00	100.00
BO2	PLGA-PEG20 NP	30	42.49	45.44	44.17	44.03
		60	55.23	55.26	53.78	54.76
		120	68.67	70.73	69.64	69.68
	PLGA-PEG-ZOL NP	30	80.60	79.97	81.08	80.55
		60	83.31	81.31	81.15	81.92
		120	100.00	100.00	100.00	100.00

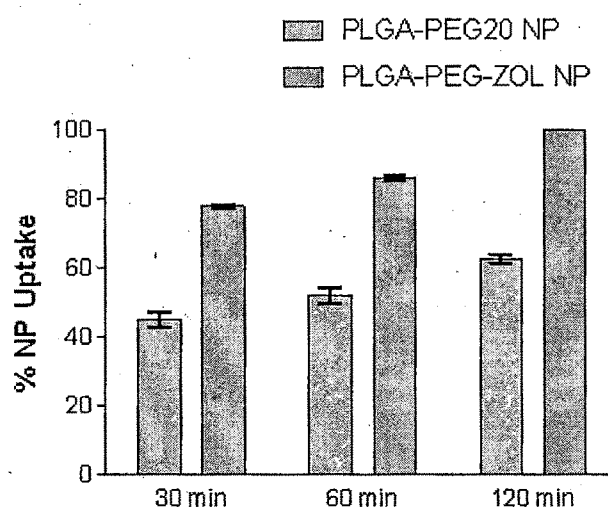


Figure 5.5: Endocytic uptake of 6-coumarin loaded PLGA-PEG20 NP and PLGA-PEG-ZOL NP in human breast cancer cell line (a) MCF7 after incubation for 30, 60 and 120 min using FACS as estimation technique. Data presented as Mean \pm SEM, n = 3.

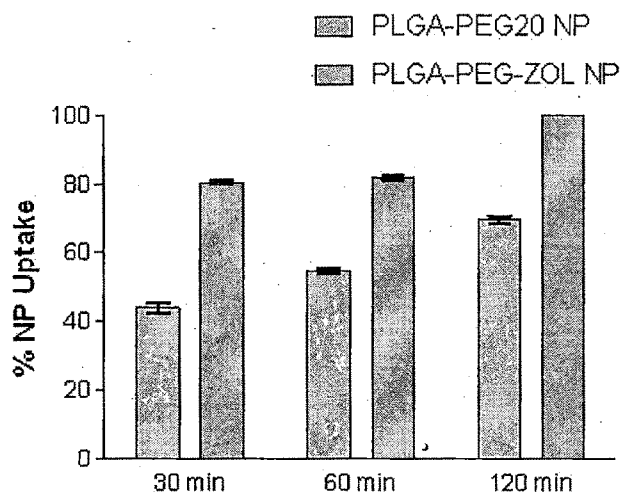


Figure 5.6: Endocytic uptake of 6-coumarin loaded PLGA-PEG20 NP and PLGA-PEG-ZOL NP in human breast cancer cell line BO2 after incubation for 30, 60 and 120 min using FACS as estimation technique. Data presented as Mean \pm SEM, n = 3.

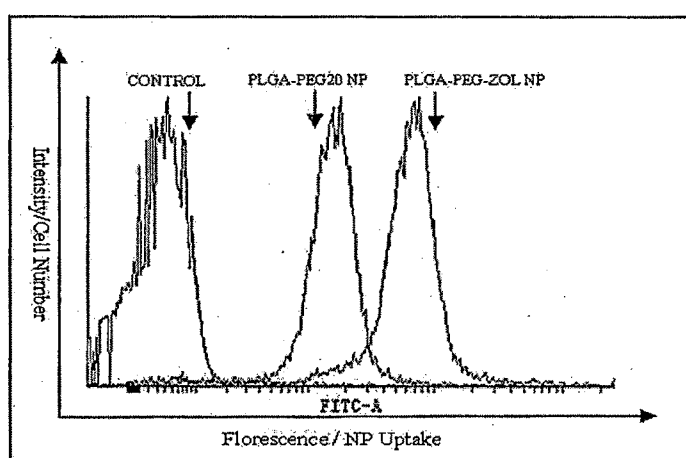


Figure 5.7: Endocytic uptake histogram of control cells, 6-coumarin loaded PLGA-PEG20 NP and PLGA-PEG-ZOL NP in human breast cancer cell line BO2 after incubation for 120 min using FACS as estimation technique.

5.5.3 PBCA NP uptake by cancer cell

The cellular uptake of PBCA-PEG NPs and PBCA-PEG-ZOL NPs were evaluated in BO2 and MCF-7 cell line. In case of MCF-7 cell line, uptake of PBCA-PEG-ZOL NPs after 30 min was found to be 82.54% which is 1.62 times higher than PBCA-PEG NPs. Internalization of PBCA-PEG-ZOL NPs reached 100% within 120 min, while only 63.92% PBCA-PEG NPs were internalized at same time point (Fig. 5.8; Table 5.4). Similar results were found when cellular uptake was studied using BO2 cell lines. Across all time points, the uptake of PBCA-PEG-ZOL NPs was found to be more than 1.4 times higher than PBCA-PEG NPs. Same way, in BO2 cell line NP uptake for PBCA-PEG20 NP was 29% less in comparison to PBCA-PEG-ZOL NP after 120 min which shows enhanced uptake because of ZOL grafting (Fig. 5.9; Table 5.4).

Table 5.4: Endocytic uptake of 6-coumarin loaded PBCA-PEG20 NP and PBCA-PEG-ZOL NP in human breast cancer cell line (a) MCF7 and (b) BO2 after incubation for 30, 60 and 120 min using FACS as estimation technique. Data presented as Mean \pm SEM, n = 3.

Cell line	Formulation	Time (min)	% cell uptake			Mean of % cell uptake
MCF7	PBCA-PEG20 NP	30	50.33	50.23	52.40	50.99
		60	49.67	59.44	57.64	55.58
		120	63.03	64.34	64.40	63.92
	PBCA-PEG-ZOL NP	30	79.21	85.51	82.92	82.55
		60	86.03	93.01	91.94	90.33
		120	100.00	100.00	100.00	100.00
BO2	PBCA-PEG20 NP	30	42.87	44.35	43.27	43.50
		60	53.27	53.87	54.72	53.95
		120	68.94	73.12	71.59	71.22
	PBCA-PEG-ZOL NP	30	62.30	64.20	64.43	63.64
		60	76.85	80.27	79.10	78.74
		120	100.00	100.00	100.00	100.00

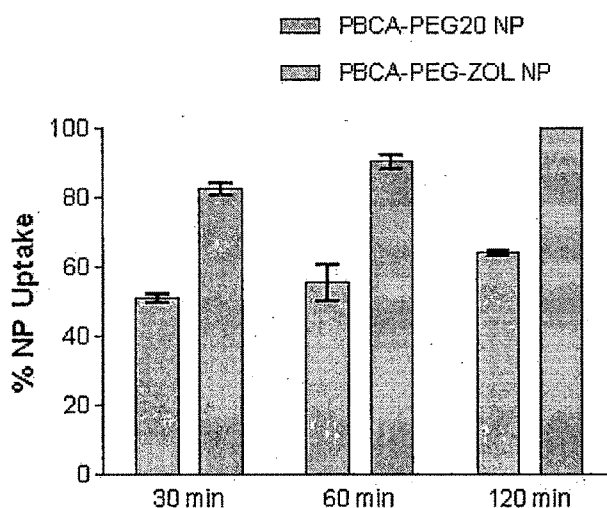


Figure 5.8: Endocytic uptake of 6-coumarin loaded PBCA-PEG20 NP and PBCA-PEG-ZOL NP in human breast cancer cell line (a) MCF7 after incubation for 30, 60 and 120 min using FACS as estimation technique. Data presented as Mean \pm SEM, n = 3.

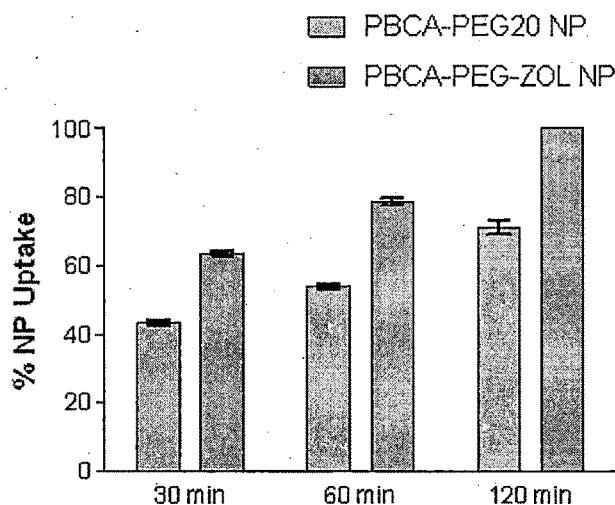


Figure 5.9: Endocytic uptake of 6-coumarin loaded PBCA-PEG20 NP and PBCA-PEG-ZOL NP in human breast cancer cell line BO2 after incubation for 30, 60 and 120 min using FACS as estimation technique. Data presented as Mean \pm SEM, n = 3.

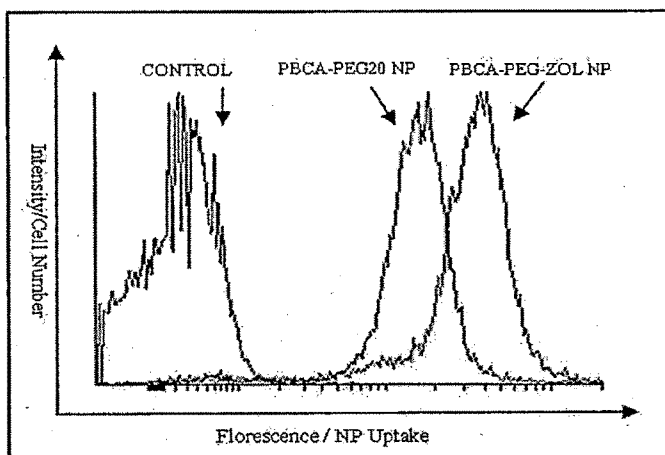


Figure 5.10: Endocytic uptake histogram of 6-coumarin loaded PBCA-PEG20 NP and PBCA-PEG-ZOL NP in human breast cancer cell line BO2 after incubation for 120 min using FACS as estimation technique.

5.6 Cell uptake route characterization

5.6.1 Introduction

The majority of targeted deliveries aim to avoid lysosomal trafficking in an effort to protect the drug molecule or biomolecules from enzymatic degradation. This issue need only be addressed for those complexes which are expected to release drug molecules prior to endosomal fusion with lysosomal contents. The endolysosomal pathway is of direct relevance to targeted intracellular drug delivery because not only does endocytosis allow for macromolecular internalization but it enables receptor- and lysosome-specific localization. Using the current knowledge of endocytic mechanisms and the key players involved, drug delivery systems can be bioengineered to exploit these pathways for more specialized intracellular delivery (Prasmickaite et al, 2002).

Endocytosis is a conserved process where extracellular nutrients are taken up into the cells usually by the invagination of cell membrane by forming vesicles. Uptake of particulate systems could occur through various processes, such as by phagocytosis, macropinocytosis, or by receptor mediated endocytosis (RME) (Foster et al, 2001, Bareford and Swaan, 2007). RME can be further classified into the classical clathrin mediated pathway and caveolae-mediated endocytosis. These various endocytic routes vary in the composition of coat, size and shape of vesicles, and fate of the

internalized material (Nam et al, 2009). The route of trafficking of NP is very important to determined destination and residence time as well as effectiveness of NP as drug delivery system. NP internalized by clathrin mediated pathway ended in lysosome or golgi through endosome and exposed to harsh environment of lysosome and reduced pH. Caveolae mediated endocytosis bypass lysosomal pathway and routed to endoplasmic reticulum or nucleus which proven very effective for intracellular therapeutic delivery (Murthy et al 2003; Bathori et al 2004).

5.6.1.1 Clathrin-dependent Receptor-mediated endocytosis

Clathrin-dependent RME is the most investigated vesicular pathway for targeted drug delivery. In addition to a well characterized internalization scheme, numerous receptors, including transferrin, asialoglycoprotein (Biessen et al, 1999), epidermal growth factor (EGF) (Mamot et al, 2003), and chemokine (Biragyn et al, 2004), serve as high affinity binding sites and have been investigated for their use in targeting to different cell types. Ligands bind specific cell surface receptors, signaling their directional movement towards clathrin underlined pits in the membrane. After binding and internalization, ligands and/or receptors may be recycled or ultimately enzymatically degraded in the lysosomal compartment depending on cellular requirements.

Peptides such as Arg–Gly–Asp (RGD) specifically bind to a cell adhesion receptor and have recently been used in targeted drug delivery systems for the treatment of cancer and autoimmune diseases (Dunehoo et al, 2006). In addition, targeted subcellular delivery to the lysosomes is achieved by carbohydrate-mediated binding and internalization via glycoreceptors allowing for intracellular delivery of recombinant enzymes in an effort to restore deficient lysosomal hydrolases (Muro et al, 2006). In the presence of a receptor recycling component, the intracellular accumulation of these targeted systems can offer prolonged drug effects for conjugated delivery systems (Muro et al, 2005).

5.6.1.2 Fluid phase endocytosis (FPE)

FPE is a nonspecific adsorptive pinocytic mechanism which allows for the cellular incorporation of molecules contained in the extracellular fluid. Molecules absorbed via this pathway avoid direct binding with membrane constituents but often possess

nonspecific charge and hydrophobic membrane interactions. This process accompanies receptor-mediated absorption, internalizing not only the receptor-ligand complexes concentrated in these pits but also extracellular fluid which is proportional to the internal volume of the endosomes, approximately 100 nm in diameter.

Cationic molecules naturally reside near the negatively charged membrane and internalize through FPE. Macromolecular drug delivery systems have been modified to take advantage of this characteristic. Positively charged hydroxypropyl methacrylamide (HPMA) polymers (Mitra et al, 2004) and poly(l-lysine) conjugates (Persiani et al, 1989) show greater accumulation in cells than negatively charged polymers. One well-characterized FPE-directed drug delivery system utilizes dextran conjugates to successfully deliver superoxide dismutase in hepatic tissue following modification of saccharides resulting in nonspecific electrostatic interactions with the cell surface (Fujita et al, 1992).

5.6.1.3 Caveolin assisted receptor mediated endocytosis

Caveolae are flask-shaped invaginations, ranging from 50 to 100 nm in diameter, making up more than 10% of the plasma membrane for endothelial cells. These invaginations are held in place by underlying actin filaments in the cytoskeleton, where certain membrane proteins are found to concentrate. Unlike clathrin mediated endocytosis, caveolae-assisted endocytosis is a triggered process that involves subsequent complex signaling.

Ligands known to be internalized through receptor-dependent caveolae-mediated endocytosis include folic acid, albumin, and cholesterol (Chang et al, 1992). Folic acid, or vitamin B9, appears an especially attractive target for targeted drug delivery. For example, folate targeted poly(ethylene glycol) (PEG)-coated nanoparticles are found to bind to folate receptors allowing for caveolae-assisted endocytosis. In addition, albumin, which interacts with endothelium by binding to albumin (gp60) receptor, is used in vascular targeting through its caveolae mediated uptake mechanism (Schnitzer et al, 2001). Caveolae-directed systems have been used to target chemotherapeutics to a nondegradative pathway, where pH sensitive bonds have allowed for drug release followed by diffusion across the endosomal membrane directed to the nucleus (Murthy et al, 2003). Characterizing the proteins and receptors

pertinent to caveolar transport will aid in the design of targeted drug carriers which bypass the harsh environment of the lysosomes to render this trafficking pathway less harmful to drug complexes (Bathori et al, 2004).

5.6.2 Protocol for NP uptake route characterization

BO2 cells were seeded on 6-well plates at the density of 1×10^5 cells per well and allowed to attach and grow. After 48 h, cells were incubated with various NP uptake route blocker listed in table 5.5 followed by treatment with 1 ml, 100 $\mu\text{g}/\text{ml}$ 6-coumarin loaded PLGA-PEG20 NPs and PLGA-PEG-ZOL NPs for 30 or 90 min. Cells were washed, harvested and analyzed in FACS (Canto-II, BD) for total amount of NPs uptake by 10,000 cells. After treatment with specific inhibitor, each well was tested for cell uptake of 6-coumarin loaded PLGA-PEG20 NPs and PLGA-PEG-ZOL NPs using FACS.

5.6.3 Cell uptake route characterization for PLGA NP

In our study we have used various cell uptake route inhibitors to determine intracellular route for NP trafficking using BO2 cell line. Treatment with sodium azide reduced NP uptake up to 90% indicating internalization mechanism was energy dependent process for both PLGA-PEG20 NP as well as PLGA-PEG-ZOL NP (Fig. 5.11; Table 5.6). Increase in concentration of both NPs from 50 to 200 $\mu\text{g}/\text{ml}$ shows reduction in fraction uptake. The trend demonstrated that the process was followed saturable kinetic and eliminate possibility of macropinocytosis uptake which follow linear uptake kinetic (Catizone et al, 1993). The size of NP is near to 100 nm that is very low in compare to threshold required for phagocytosis activation usually that happen above 1 μm (Rupper and Cardelli, 2001). After treatment of BO2 cell line with wortmanin (micropinocytosis inhibitor) we found no significant change in PLGA-PEG20 NP and PLGA-PEG-ZOL NP uptake and that confirmed the presence of non-micropinocytosis pathway. In case of genistein treatment (caveolae-mediated endocytosis inhibitor), PLGA-PEG20 NP demonstrated 90.6% uptake while PLGA-PEG-ZOL NP shows 79.5% uptake. After treatment with phenyl arsinoxide (clathrin mediated endocytosis inhibitor), PLGA-PEG20 NP demonstrated only 25.2% uptake while PLGA-PEG-ZOL NP show 65.6% uptake. But after treatment with both genistein and phenyl arsinoxide the PLGA-PEG-ZOL NP uptake was reduced dramatically to 15.5%. PLGA-PEG-ZOL NP uptake can be block by using both

inhibitor simultaneously but not by individual, thus it display that PLGA-PEG-ZOL NP uptake routed by both clathrin mediated and caveolae mediated endocytosis where one pathway compensate NP uptake when second pathway got blocked.

Table 5.5: Inhibitors of cellular uptake of NP and its concentration used for cell culture.

Inhibitor	Conc.	Action on endocytosis route
Sodium azide	10 mM	All energy dependant endocytosis inhibition
Wortmamin	10 μ M	Macropinocytosis inhibition
Phenyl arsine oxide	10 μ M	Clathrin type endocytosis inhibition
Genistein	200 μ M	caveola type endocytosis inhibition

Table 5.6: Characterization of route for NP uptake using various endocytosis inhibitors on BO2 cell line and 6-coumarin loaded PLGA-PEG-20 NP and PLGA-PEG-ZOL NP. Data presented as Mean \pm SEM, n = 3.

Formulation	Treatment with Inhibitor	% cell uptake			Mean % cell Up take
PLGA-PEG20 NP	CONTROL	100.00	100.00	100.00	100.00
	SODIUM AZIDE	9.34	9.05	20.32	12.90
	WORTMANIN	94.10	103.51	105.46	101.02
	PHENYL ARSINOXIDE	25.46	29.57	17.56	24.20
	GENISTEIN	90.56	88.74	92.53	90.61
	GENISTEIN & PHENYL ARSINOXIDE	28.62	22.64	17.75	23.00
PLGA-PEG-ZOL NP	CONTROL	100.00	100.00	100.00	100.00
	SODIUM AZIDE	10.24	9.04	12.35	10.54
	WORTMANIN	96.47	101.25	115.72	104.48
	PHENYL ARSINOXIDE	65.72	66.21	64.84	65.59
	GENISTEIN	80.14	74.30	83.99	79.47
	GENISTEIN & PHENYL ARSINOXIDE	19.15	19.10	8.22	15.49

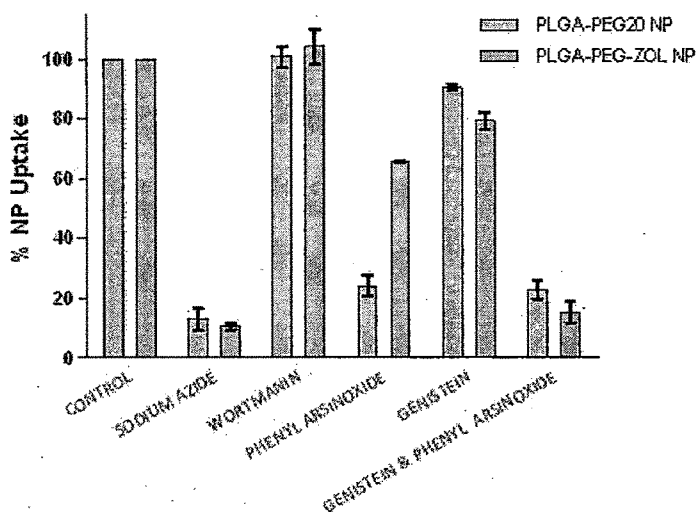


Figure 5.11: Characterization of route for NP uptake using various endocytosis inhibitors on BO2 cell line and 6-coumarin loaded PLGA-PEG-20 NP and PLGA-PEG-ZOL NP. Data presented as Mean \pm SEM, n = 3.

5.6.4 Cell uptake route characterization for PBCA NP

After treatment of BO2 cell line with wortmanin (micropinocytosis inhibitor) there was no significant change in PBCA-PEG20 NP and PBCA-PEG-ZOL NP uptake and that confirmed the presence of non-micropinocytosis pathway (Fig. 12; Table 7). In case of genistein treatment (caveolae-mediated endocytosis inhibitor), PBCA-PEG20 NP demonstrated 80.94% uptake while PBCA-PEG-ZOL NP shows 70.87% uptake. After treatment with phenyl arsinoxide (clathrin mediated endocytosis inhibitor), PBCA-PEG20 NP demonstrated 80.16% uptake while PBCA-PEG-ZOL NP show 65.38% uptake. But after treatment with both genistein and phenyl arsinoxide the PBCA-PEG-ZOL NP uptake was reduced dramatically to 33% (Fig. 12; Table 7), while PBCA-PEG-ZOL NP shown 14.28 % uptake. Result demonstrated that PBCA-PEG-ZOL NP uptake was reduce but can't block completely by using both inhibitor simultaneously or by individual, thus it display that PBCA-PEG-ZOL NP uptake routed by both clathrin mediated and caveolae mediated endocytosis, but there is chance of involvement of other pathway as well.

Table 5.7: Characterization of route for NP uptake using various endocytosis inhibitors on BO2 cell line and 6-coumarin loaded PBCA-PEG-20 NP and PBCA-PEG-ZOL NP. Data presented as Mean \pm SEM, n = 3.

Formulation	Treatment with Inhibitor	% cell uptake			Mean % cell Up take
PBCA-PEG20 NP	CONTROL	100.00	100.00	100.00	100.00
	SODIUM AZIDE	14.25	10.24	12.66	12.38
	WORTMANIN	102.53	96.65	94.43	97.87
	PHENYL ARSINOXIDE	82.79	76.46	81.22	80.16
	GENISTEIN	76.56	84.64	81.61	80.94
	GENISTEIN & PHENYL ARSINOXIDE	13.65	17.65	11.54	14.28
PBCA-PEG-ZOL NP	CONTROL	100.00	100.00	100.00	100.00
	SODIUM AZIDE	14.34	12.81	5.92	11.02
	WORTMANIN	107.82	94.44	103.94	102.07
	PHENYL ARSINOXIDE	66.62	63.52	66.01	65.38
	GENISTEIN	67.74	71.24	73.64	70.87
	GENISTEIN & PHENYL ARSINOXIDE	31.81	30.79	36.38	33.00

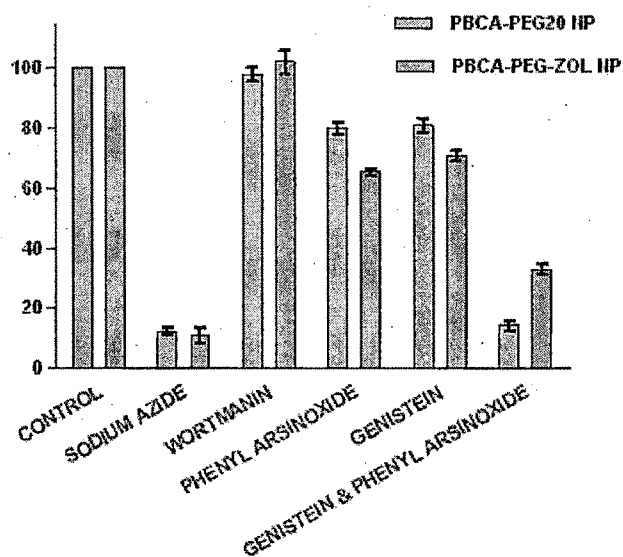


Figure 5.12: Characterization of route for NP uptake using various endocytosis inhibitors on BO2 cell line and 6-coumarin loaded PBCA-PEG-20 NP and PBCA-PEG-ZOL NP. Data presented as Mean \pm SEM, n = 3.

5.6.5 Microscopy for endosomal-lysosomal association

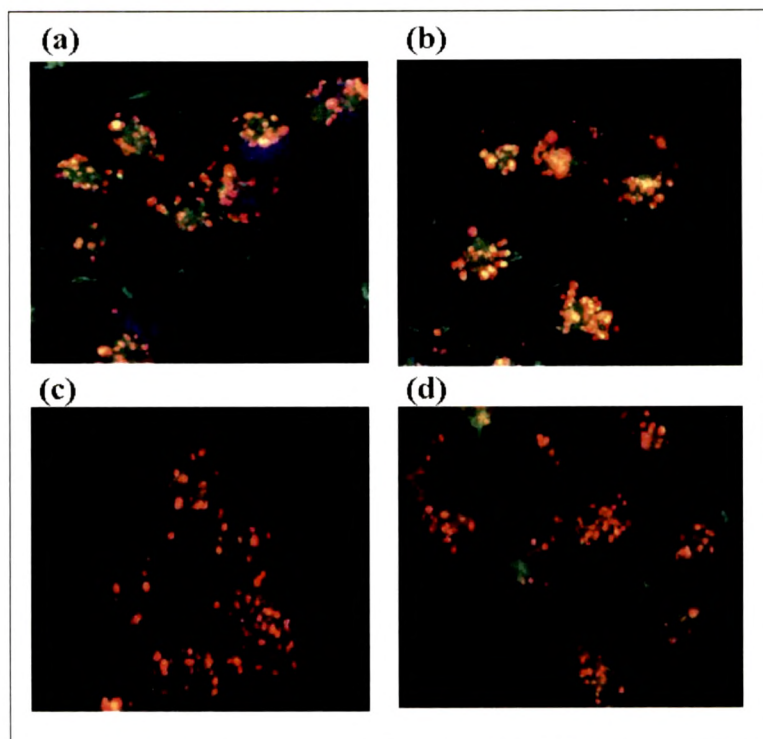


Figure 5.13: Confocal microscopic evaluation of NPs up take of PLGA-PEG20 NP and PLGA-PEG-ZOL NP using LysoTracker Red[®] and Hoechst 33342. Figure (a & b) shown overlapping images for PLGA-PEG20 NP and (c & d) shown overlapping images for PLGA-PEG-ZOL NP. Yellow color indicated NP in lysosomal compartment.

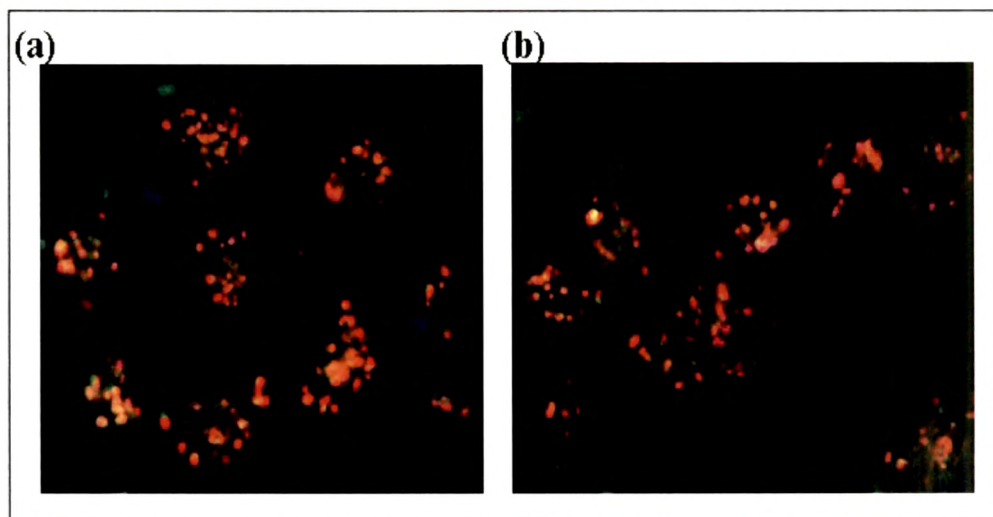


Figure 5.14: Confocal microscopic evaluation of NPs up take of PBCA-PEG20 NP and PBCA-PEG-ZOL NP using LysoTracker Red[®] and Hoechst 33342. Figure (a) shown overlapping images for PBCA-PEG20 NP and (b) shown overlapping images for PBCA-PEG-ZOL NP. Yellow color indicated NP in lysosomal compartment.

Understanding the intracellular trafficking through the endolysosomal pathway and the fate of NPs with respect to their uptake mechanism is crucial in understanding fate of NP intracellularly. Unfortunately, determination of the exact intracellular trafficking pathway of NPs is difficult due to the fast dynamics of maturation and unnoticeable morphological changes between endosomal and lysosomal compartments. To track PLGA-PEG20 NP and PLGA-PEG-ZOL NP following their uptake, the lysosomes of BO2 cell line was stained with the LysoTracker Red probe after treatment with 6-coumarin loaded PLGA-PEG20 NP and PLGA-PEG-ZOL NP. The cell nucleus was labeled with Hoechst 33342. The intracellular localization of the PLGA-PEG20 NP and PLGA-PEG-ZOL NP were traced after 120 min incubation (Fig. 5.13). Here, the colocalization of green fluorescence 6-coumarin loaded NPs with red fluorescence lysosomes produced a yellow fluorescence after merging images. Images clearly showed the colocalization of PLGA-PEG20 NP with lysosomal vesicles in cells, but the colocalization is rare in PLGA-PEG-ZOL NP treated cells. Results showed high degree of relevance with route characterization results where PLGA-PEG-ZOL NP found with very few colocalization demonstrated that NPs got endocytosis by both clathrin mediated and caveolae mediated endocytosis mechanism where caveolae pathway follow non-lysosomal route. PLGA-PEG20 NP follows predominantly to lysosome through early endosomes which displayed significant colocalization of NPs with lysosomes.

The intracellular localization of the PBCA-PEG20 NPs and PBCA-PEG-ZOL NPs were traced after 120 min incubation (Fig. 5.14). The colocalization of the green fluorescence of 6-coumarin loaded NPs, with the red fluorescence from lysosomes produced a yellow fluorescence, after merging the images. Images showed few co-localization of PBCA-PEG20 NPs with the lysosomes, but the co-localization was rare in PBCA-PEG-ZOL NPs treated cells. These results were in relevance with the route characterization results in which PBCA-PEG-ZOL NPs was less co-localization. These demonstrates that NPs were endocytosed by both clathrin mediated and

caveolae mediated endocytosis mechanism, where caveolae pathway followed a non-lysosomal route. PBCA-PEG20 NPs followed to lysosome through early endosomes which displayed few co-localization of NPs and lysosomes. However, PBCA-PEG-ZOL NP show slight co-localization and route followed was less dependent on clathrin mediated endocytosis in comparison to PBCA-PEG20 NPs.

5.7 Intracellular residence of NP

For rational drug delivery, NP residence for extended time in intracellular domain has significant role on therapeutic benefit. Although, earlier studies show that along with endocytosis, exocytosis of NP is also very fast process and start escaping internalized cargo. Therefore, when the NPs were present in the external medium, NPs transported into and out of the cell repeatedly. When NPs were removed from the external media, concentration of NPs in extracellular domain of the cell drop and the recycling equilibrium got disturb, resulting sharp reduction in intracellular NP levels (Chithrani and Chan, 2007).

5.7.1 Protocol for intracellular residence

BO2 cells were seeded on 6 well plates at the density of 1×10^5 cells per well and allowed to attach and grow. After 48 h, cells were incubated with 1ml, 100 $\mu\text{g/ml}$ 6-coumarin loaded PLGA-PEG20 NPs and PLGA-PEG-ZOL NPs for 90 min. After incubation of NP with cells, each well was washed with HBSS and incubated with 2 ml fresh HBSS. After 60, 120, 240 min time interval, cells were washed, harvested and analysed in FACS (Canto-II, BD) for total amount of NP retained in 10,000 cells.

5.7.2 Intracellular residence of PLGA NP with time

NPs residence time inside the cells is usually depend on intracellular route taken by the NPs. Depending on internalization mechanism there are three different ways possible for NPs as illustrated in Fig 5.15. More residence time inside the cell gives enough time for NPs to release drug in cytoplasm and very important especially when intracellular delivery of therapeutic agents is desirable (Panyam and Labhasetwar, 2003). In experiment, as soon as NP media removed and replaced with fresh media, the NPs were started escaping at varying rate with different formulations. The concentration of NPs in external media had slight effect on fraction of NP escape with time. Treatment with sodium azide (10mM) and incubation at 4°C successfully block

NP escape demonstrated energy dependent process of exocytosis. % NP retention with time was carried out for PLGA-PEG20 NP and PLGA-PEG-ZOL NP. Results demonstrated that after 60 min, % retention of PLGA-PEG-ZOL NP in BO2 cell line was found 24.38% more in comparison to PLGA-PEG20 NP (Fig. 5.16; Table 5.8). Retention of PLGA-PEG-ZOL NP after 120 min and 240 min was found 16.4% and 18.32% higher than PLGA-PEG20 NP (Fig. 5.16; Table 5.8). From result, it could be confirmed that PLGA-PEG-ZOL NP might follow different route of intracellular trafficking which prolong it's time for getting exocytosis from BO2 cells.

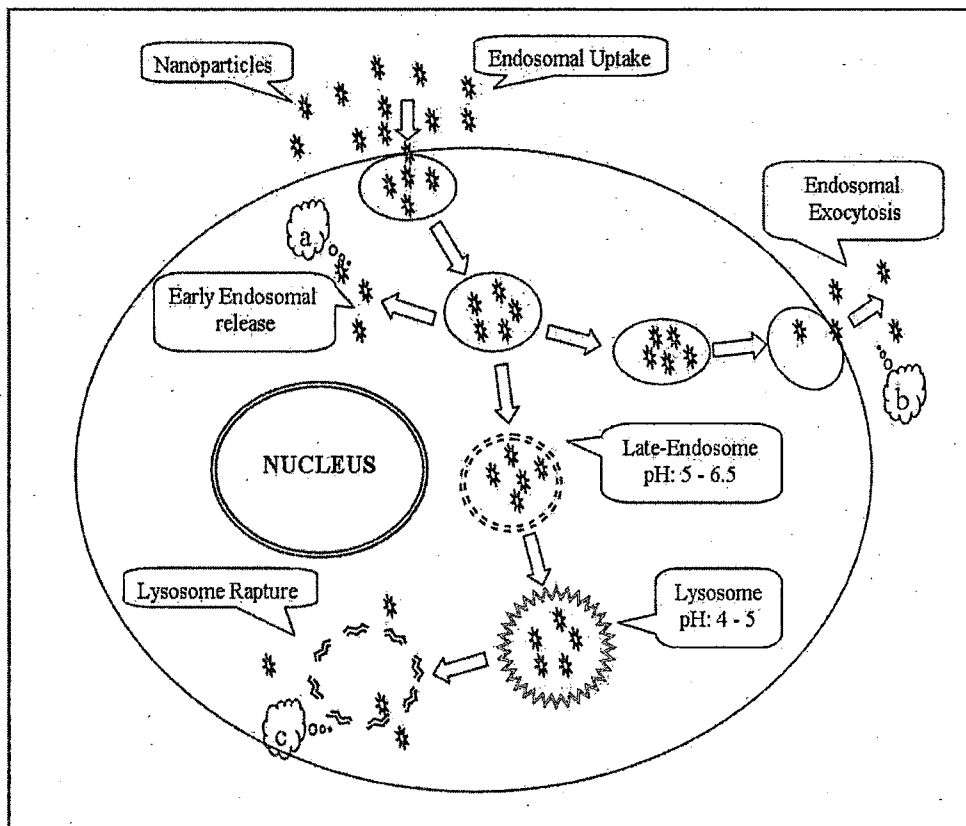


Figure 5.15: Intracellular association of NPs with endosome-lysosome compartments and possible route of trafficking. (a) Early endosomal release - route without involvement of lysosome (b) Immediate endosomal exocytosis (c) Late endosome-lysosome association and release by lysosome rapture.

Table 5.8: PLGA-PEG20 NP and PLGA-PEG-ZOL NP retention time in intracellular compartment after uptake in BO2 cell line after incubation for control, 60, 120 and 240 min using FACS as estimation technique. Data presented as Mean \pm SEM, n = 3.

Formulation	Time (min)	% cell uptake			Mean of % cell uptake
PLGA-PEG20 NP	0	100.00	100.00	100.00	100.00
	60	52.22	48.96	34.08	45.09
	120	22.35	21.97	15.29	19.87
	240	12.63	11.94	7.96	10.84
PLGA-PEG-ZOL NP	0	100.00	100.00	100.00	100.00
	60	68.47	70.02	69.92	69.47
	120	33.80	36.80	38.21	36.27
	240	31.01	28.01	28.46	29.16

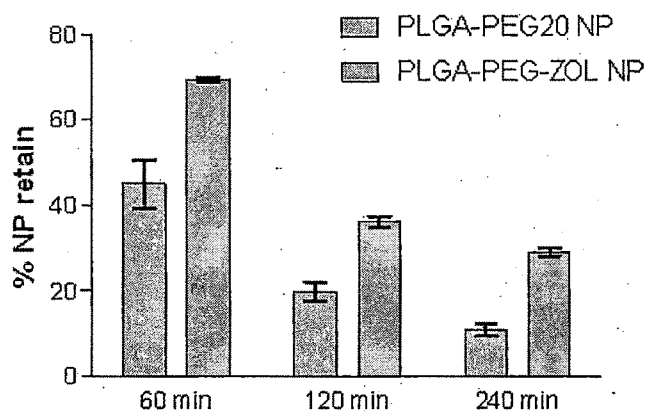


Figure 5.16: PLGA-PEG20 NP and PLGA-PEG-ZOL NP retention time in intracellular compartment after uptake in BO2 cell line after incubation for control, 60, 120 and 240 min using FACS as estimation technique. Data presented as Mean \pm SEM, n = 3.

5.7.3 Intracellular residence of PBCA NP with time

% NP retention with time was also carried out for PBCA-PEG20 NP and PBCA-PEG-ZOL NP in BO2 cell line. Results demonstrated that after 60 min, % retention of PBCA-PEG-ZOL NP in BO2 cell line was found 49.15% in comparison to PBCA-PEG20 NP having 24.14% NP remaining intracellularly (Fig. 17; Table 5.9). Retention of PBCA-PEG-ZOL NP after 120 min and 240 min was found 32.17% and 26.62% while the respective amount for PBCA-PEG20 NP was 14.41 % and 8.72 % (Fig. 17; Table 5.9). From result, it could be confirmed that ZOL anchored NP might have nondegradative pathway or have interaction with intracellular organelles responsible for retention.

Table 5.9: PBCA-PEG20 NP and PBCA-PEG-ZOL NP retention time in intracellular compartment after uptake in BO2 cell line after incubation for control, 60, 120 and 240 min using FACS as estimation technique. Data presented as Mean \pm SEM, n = 3.

Formulation	Time (min)	% cell uptake			Mean of % cell uptake
PBCA-PEG20 NP	0	100.00	100.00	100.00	100.00
	60	21.37	25.00	26.04	24.14
	120	12.76	16.20	14.29	14.41
	240	9.41	8.98	7.78	8.72
PBCA-PEG-ZOL NP	0	100.00	100.00	100.00	100.00
	60	52.23	45.86	49.36	49.15
	120	32.39	33.91	30.21	32.17
	240	30.77	26.97	22.13	26.62

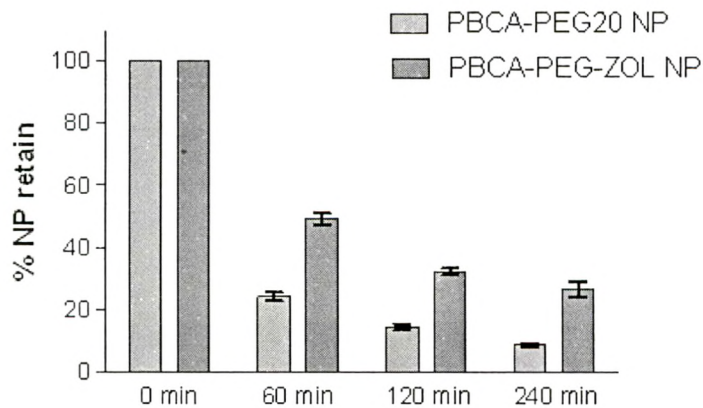


Figure 5.17: PBCA-PEG20 NP and PBCA-PEG-ZOL NP retention time in intracellular compartment after uptake in BO2 cell line after incubation for control, 60, 120 and 240 min using FACS as estimation technique. Data presented as Mean \pm SEM, n = 3.

5.8 Cytotoxicity by MTT assay

The MTT (3-(4,5-dimethylthiazole-2-yl)-2,5-diphenyltetrazoliumbromide) and the ATP (adenosine triphosphate) assays are widespread methods to assess cell viability. MTT is reduced by mitochondrial dehydrogenases in living cells to a blue-magenta colored formazan precipitate. The absorption of dissolved formazan in the visible region correlates with the number of intact alive cells. Cytotoxic compounds are able to damage and destroy cells, and thus decrease the reduction of MTT to formazan (Mosmann, 1983).

One remarkable disadvantage of the MTT assay is that damaged mitochondria may still be able to reduce MTT to formazan (Sieuwerts et al, 1995). This could lead to a rightward shift of the concentration-response (absorption) curves. Damaged mitochondria could further evolve from sharp formazan crystals/needles and alter the reduction of MTT to formazan. Thus, the formation of cell/mitochondria damaging formazan needles was prevented by microscopic supervision of needle formation and led to an optimized incubation time for MTT of 50-70 min. Furthermore, more than 1 enzyme involved in oxidative/reductive metabolism may play a role in the reduction of MTT to formazan (Loveland et al, 1992). However, this study revealed that these potential problems did not alter IC₅₀ values in a significant manner, as the PCAs showed inter-correlation of the results of the 3 cell viability assays. The development of the MTT assay as a homogeneous assay was, however, a major achievement since washing steps during the MTT assay were associated with the loss of less attached damaged and living cells leading to a higher degree of variation.

5.8.1 Protocol for cytotoxicity assay of formulation using MTT assay

The effect of DTX, DTX in combination with ZOL, DTX loaded PLGA NPs, PLGA-PEG NPs and PLGA-PEG-ZOL NPs on cell proliferation was determined by MTT based colorimetric assay (Sahoo and Labhasetwar, 2005). Cells were plated onto 96-well, flat-bottomed plates at 5000 cells per well. After incubation of 24 h at 37°C,

medium was removed and treated with 200 μ l medium containing varying concentrations of DTX, DTX-ZOL, DTX loaded PLGA-PEG NPs and PLGA-PEG-ZOL NPs ranging from 0.5, 2 and 8 nM/ml for 48 and 72 h. After 48 h and 72 h, medium was removed, replaced with medium containing 100 μ l MTT (500 μ g/ml) and incubated. After 1 h, 100 μ l SDS solution (20% w/v, Water: DMF in 1:1 ratio, pH 4.7) was added and further incubated for 24 h to dissolve formazan crystals. Relative percentage of metabolically active cells to untreated control was determined on the basis of the mitochondrial conversion of MTT to formazan. The amount of MTT that is converted to formazan indicates the number of viable cells. The results were assessed in a 96-well format ELISA plate reader (Victor 1420, PerkinElmer) by measuring the absorbance at a wavelength of 570 nm. The IC₅₀ was determined by nonlinear regression analysis using the equation for a sigmoid plot (Jain et al. 2008).

5.8.2 Cytotoxicity assay of PLGA NP

Cytotoxicity curve and IC₅₀ value were determined for different conjugated and unconjugated nanoparticulate formulations (DTX loaded PLGA-PEG NPs and PLGA-PEG-ZOL NPs) and further compared with DTX solution and DTX-ZOL mixture in dose dependent and time dependent manner in BO2 and MCF7 cell lines using MTT assay (Mosmann T, 1983). IC₅₀ value, concentration of drug required for 50% cell death, is listed in Table 5.14. From results, it is observed that PLGA-PEG-ZOL NPs exhibited significantly higher cytotoxicity compared to DTX, DTX-ZOL and unconjugated NPs at all drug concentrations and time points in both cell lines. The IC₅₀ value for BO2 cells treated with PLGA-PEG-ZOL NPs was found to be 1.06 nM after 48 h that was 5.45 and 2.84 times less than DTX, DTX loaded PLGA-PEG NPs respectively (Table 5.14, fig. 5.19). Exposure for 72 h further lowered the IC₅₀ value by 1/3rd of its value to 0.32, which was more than 10 times less in comparison with DTX solution. Incubation of MCF7 cells with PLGA-PEG-ZOL NPs also resulted in enhanced cytotoxic effects when compared with DTX and unconjugated NP formulations (Table 5.14, fig. 5.20). When IC₅₀ values for BO2 cells are compared with that of MCF 7 cells, about 1.55 times higher concentration of PLGA-PEG-ZOL NPs was required in MCF 7 cells after 48 h and 72 h (Table 5.14, fig. 5.21). Therapeutic efficacy of drug loaded targeted NPs depends on cellular uptake, intracellular distribution, and more importantly the amount of drug available from the internalized NPs inside the cell (Acharya et al. 2009). The enhanced cytotoxic effect

of PLGA-PEG-ZOL NPs could be attributed by higher uptake via ZOL mediated endocytosis. PLGA-PEG-ZOL NPs found more active in BO2 cells demonstrated high efficiency of ZOL toward cancer cells having morphology similar to bone (Table 5.14, fig. 5.22).

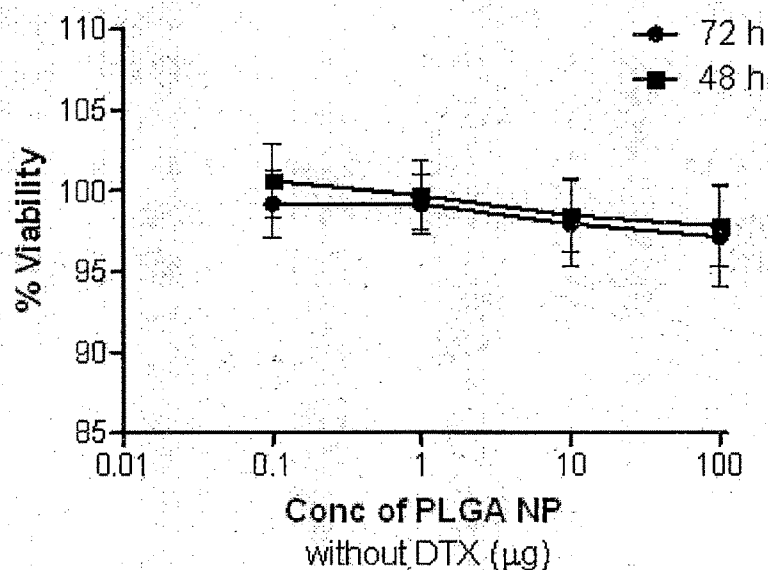


Figure 5.18: Cytotoxicity study PBCA NP without DTX in MCF7 after 48 h and 72 h using MTT assay. Data presented as Mean \pm SEM, n = 3.

Table 5.10: Cytotoxicity study of DTX solution, ZOL-DTX solution, DTX loaded PLGA-PEG20 NP and PLGA-PEG-ZOL NP in MCF7 after 48 h using MTT assay. Data presented as Mean \pm SEM, n = 3.

Cell line/ time	Formulation	Conc of DTX (nM)	% Viability			Mean of % viability
MCF7/ 48 h	DTX	0.5	92.49	106.07	102.67	100.41
		2	60.27	64.85	74.16	66.43
		8	38.00	45.35	45.86	43.07
	DTX-ZOL	0.5	91.84	89.55	94.38	91.92
		2	62.67	62.33	73.03	66.01
		8	43.62	42.76	51.04	45.81

	PLGA- PEG20 NP	0.5	72.81	76.80	76.07	75.22
		2	49.11	56.08	62.52	55.91
		8	34.07	36.35	48.00	39.48
	PLGA- PEG-ZOL NP	0.5	52.90	59.61	60.25	57.58
		2	35.97	48.63	47.14	43.91
		8	30.77	33.40	37.80	33.99

Table 5.11: Cytotoxicity study of DTX solution, ZOL-DTX solution, DTX loaded PLGA-PEG20 NP and PLGA-PEG-ZOL NP in MCF7 after 72 h using MTT assay. Data presented as Mean \pm SEM, n = 3.

Cell line/ time	Formulation	Conc of DTX (nM)	% Viability			Mean of % viability
MCF7/ 72 h	DTX	0.5	84.31	89.07	84.37	85.92
		2	50.05	64.18	77.56	63.93
		8	30.18	33.03	37.96	33.73
	DTX-ZOL	0.5	82.52	78.37	82.24	81.05
		2	47.63	54.02	76.96	59.54
		8	31.37	27.63	42.90	33.97
	PLGA-PEG20 NP	0.5	60.06	61.03	82.64	67.91
		2	39.86	49.00	68.25	52.37
		8	24.53	27.43	36.66	29.54
	PLGA-PEG- ZOL NP	0.5	37.97	51.61	63.01	50.86
		2	23.17	30.63	54.47	36.09
		8	19.66	26.40	27.69	24.58

Table 5.12: Cytotoxicity study of DTX solution, ZOL-DTX solution, DTX loaded PLGA-PEG20 NP and PLGA-PEG-ZOL NP in BO2 cell line after 48 h using MTT assay. Data presented as Mean \pm SEM, n = 3.

Cell line/ time	Formulation	Conc of DTX (nM)	% Viability			Mean of % viability
BO2/	DTX	0.5	99.63	105.41	96.05	100.36

48 h		2	54.71	63.43	60.31	59.48
		8	32.60	44.20	36.91	37.90
	DTX-ZOL	0.5	98.69	107.12	92.91	99.57
		2	57.36	66.37	58.35	60.69
		8	36.88	46.02	38.61	40.50
	PLGA-PEG20 NP	0.5	61.11	72.90	72.28	68.76
		2	41.04	49.59	45.95	45.53
		8	24.47	39.43	23.01	28.97
	PLGA-PEG-ZOL NP	0.5	55.30	63.59	55.87	58.25
		2	35.49	44.50	37.14	39.05
		8	21.64	36.16	23.76	27.19

Table 5.13: Cytotoxicity study of DTX solution, ZOL-DTX solution, DTX loaded PLGA-PEG20 NP and PLGA-PEG-ZOL NP in BO2 cell line after 72 h using MTT assay. Data presented as Mean \pm SEM, n = 3.

Cell line/ time	Formulation	Conc of DTX (nM)	% Viability			Mean of % viability
BO2/ 72 h	DTX	0.5	88.02	87.02	83.87	86.30
		2	36.52	36.52	43.14	38.72
		8	21.66	21.66	24.17	22.50
	DTX-ZOL	0.5	87.83	85.83	83.68	85.78
		2	35.98	35.35	40.47	37.27
		8	20.85	20.31	24.38	21.85
	PLGA-PEG20 NP	0.5	58.34	58.76	67.83	61.64
		2	29.09	35.64	36.91	33.88
		8	15.73	15.16	15.25	15.38
	PLGA-PEG- ZOL NP	0.5	40.34	44.18	49.90	44.81
		2	25.25	14.96	24.24	21.48
		8	12.65	12.29	14.52	13.15

Table 5.14: Cytotoxicity study of DTX solution, ZOL-DTX solution, DTX loaded PLGA-PEG20 NP and PLGA-PEG-ZOL NP in MCF7 and BO2 cell line after 48 h and 72 h using MTT assay.

Condition	DTX	DTX-ZOL	PLGA-PEG20 NP	PLGA-PEG-ZOL NP
MCF7 48 hrs	6.54	6.84	2.76	1.7
MCF7 72 hrs	5.23	4.93	1.35	0.49
BO2 48 hrs	5.78	6.08	3.01	1.06
BO2 72 hrs	3.39	3.24	0.48	0.32

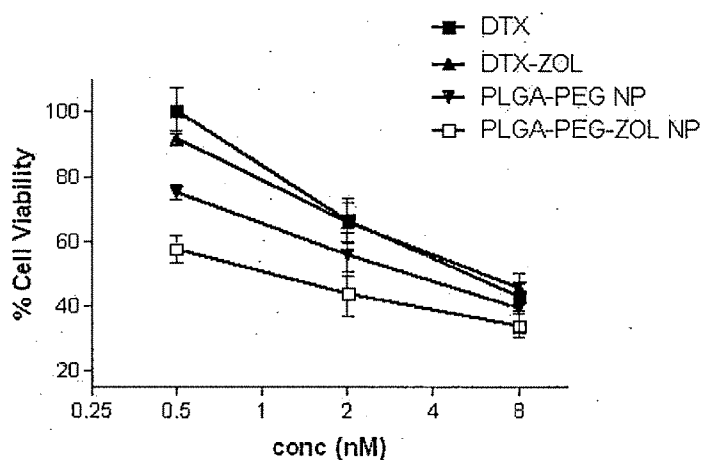
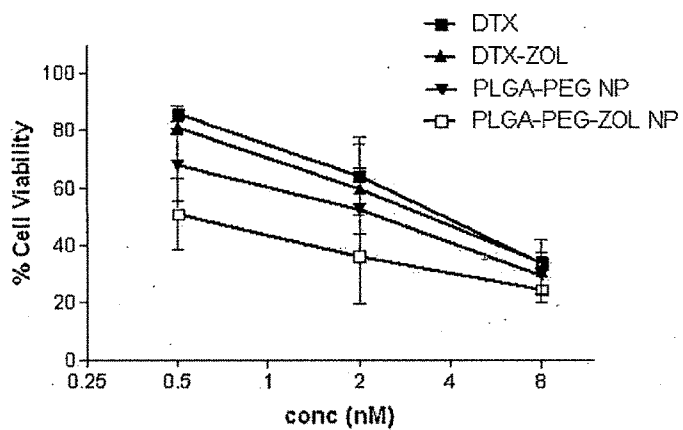
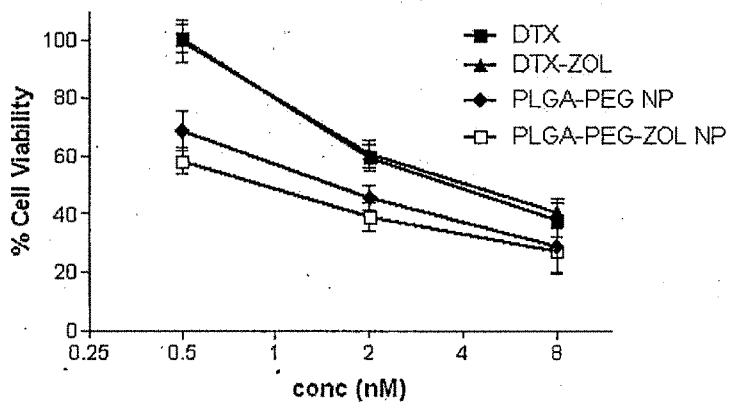


Figure 5.19: Cytotoxicity study of DTX solution, ZOL-DTX solution, DTX loaded PLGA-PEG20 NP and PLGA-PEG-ZOL NP in MCF7 cell line after 48 h using MTT assay. Data presented as Mean \pm SEM, n = 3.



F

F



F

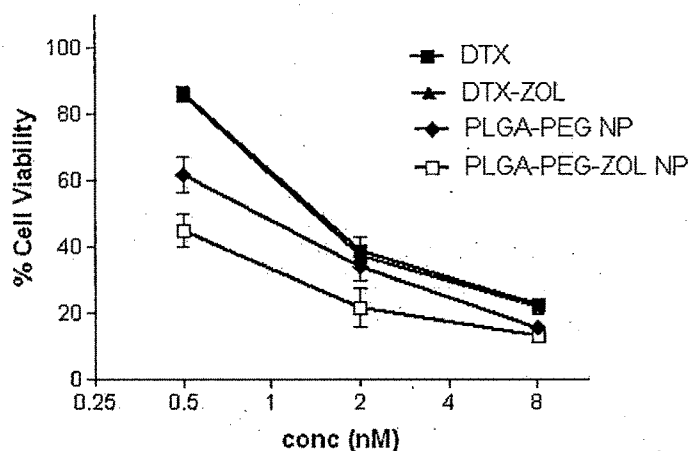


Figure 5.22: Cytotoxicity study of DTX solution, ZOL-DTX solution, DTX loaded PLGA-PEG20 NP and PLGA-PEG-ZOL NP in BO2 cell line after 72 h using MTT assay. Data presented as Mean \pm SEM, n = 3.

5.8.3 Cytotoxicity assay of PBCA NP

The therapeutic potentialities of different conjugated and unconjugated nanoparticulate formulations (DTX loaded PBCA-PEG NPs and PBCA-PEG-ZOL NPs) were compared with DTX solution and DTX-ZOL mixture in dose dependent and time dependent manner in MCF-7 and BO2 cell lines using MTT based cell proliferation assay (Mosmann, 1983). From results it was observed that no cytotoxicity was observed in case of cells treated with same concentration of blank PBCA-PEG NPs as that of PBCA-PEG-ZOL NPs (Fig. 5.23). PBCA-PEG-ZOL NPs exhibited significantly very lower IC_{50} values as compared to DTX, DTX-ZOL mixture and PBCA-PEG NPs across all time points in both cell lines. The IC_{50} values of PBCA-PEG-ZOL NPs were found to be approximately 10 times lower than that of DTX and DTX-ZOL mixture after 72 h of incubation in both cell lines.

The IC_{50} value for MCF-7 cells treated with PBCA-PEG-ZOL NPs was found to be 2.49 nM after 48 h that was 2.6, 2.7 and 1.4 times less than DTX, DTX-ZOL and PBCA-PEG NPs respectively (Table 5.20, Fig. 5.24). Exposure for 72 h further lowered the IC_{50} value by $1/5^{th}$ of its value to 0.46, which was more than 11 times less

in comparison with DTX solution (Table 5.20, Fig. 5.25). Incubation of BO2 cells with PBCA-PEG-ZOL NPs also resulted in enhanced cytotoxic effects when compared with DTX and unconjugated NPs formulations. The IC_{50} value for BO2 cells treated with PBCA-PEG-ZOL NPs was found to be 0.36 nM after 72 h which was 9.4, 9.0 and 7.2 times less than DTX, DTX-ZOL and PBCA-PEG NPs (Table 5.20, Fig. 5.27). There was significant decrease to about 5 and 6 times in IC_{50} values for MCF-7 and BO2 cell lines, respectively when compared with unconjugated formulations at two different time points. This significant difference in IC_{50} values of unconjugated NPs and ZOL conjugated NPs at 48 h and 72 h of exposure in MCF-7 and BO2 cells clearly indicates that the higher cytotoxic effect of PBCA-PEG-ZOL NPs in cell lines is mediated by surface functionalization of NPs with ZOL. PBCA-PEG-ZOL NPs were found to be more toxic to BO2 cells when compared with MCF-7 cells.

It was demonstrated by Panyam et al that NPs rapidly escape the endolysosomes and enter the cytoplasm (Panyam et al., 2002). The fractions of NPs that escape the endosomes seem to remain in the cytoplasm and release the encapsulated drug in a sustained manner (Sahoo et al., 2005). Thus, it can be speculated that the antitumor mechanism of PBCA-PEG-ZOL NPs is through their binding and getting internalized into tumor cells with subsequent intracellular release of DTX after PBCA degradation (Mo and Lim, 2005). Hence, we can conclude that drug loaded NPs have enhanced therapeutic efficacy when compared to drug solution. However, in this study we found that conjugation of ligand to NPs further enhances its therapeutic effectiveness to a higher level in comparison to drug solution, drug-ligand mixture and unconjugated NPs. These findings were in accordance to work performed by Mondal et al. (Mondal et al., 2010).

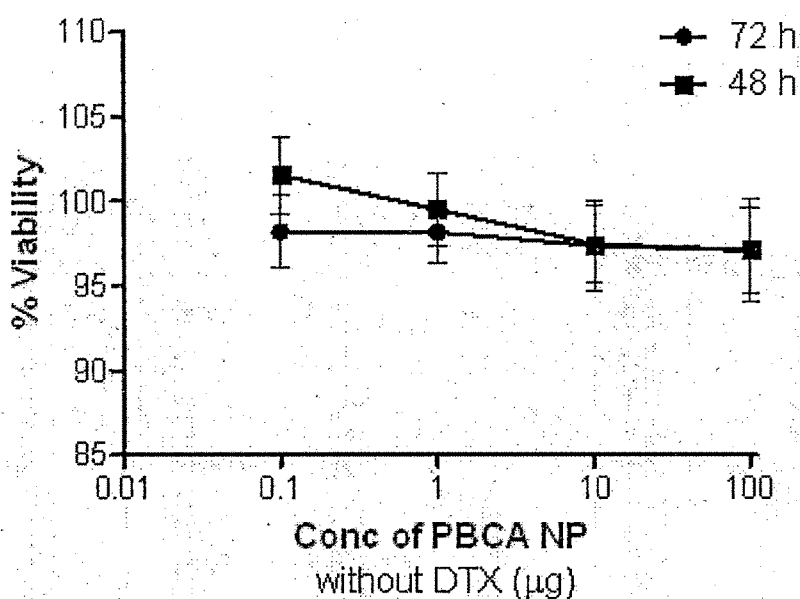


Figure 5.23: Cytotoxicity study PBCA NP without DTX in MCF7 after 48 h and 72 h using MTT assay. Data presented as Mean \pm SEM, n = 3.

Table 5.15: Cytotoxicity study of DTX solution, ZOL-DTX solution, DTX loaded PBCA-PEG20 NP and PBCA-PEG-ZOL NP in MCF7 after 48 h using MTT assay. Data presented as Mean \pm SEM, n = 3.

Cell line/ time	Formulation	Conc of DTX (nM)	% Viability			Mean of % viability
MCF7/ 48 h	DTX	0.5	92.49	106.07	102.67	100.41
		2	60.27	64.85	74.16	66.43
		8	38.00	45.35	45.86	43.07
	DTX-ZOL	0.5	91.84	89.55	94.38	91.92
		2	62.67	62.33	73.03	66.01
		8	43.62	42.76	51.04	45.81
	PLGA- PEG20 NP	0.5	70.18	65.45	72.97	69.53
		2	49.47	47.08	50.35	48.97
		8	34.05	31.21	31.01	32.09
	PLGA-	0.5	56.42	51.68	56.33	54.81

	PEG-ZOL	2	35.43	38.45	39.19	37.69
	NP	8	28.22	31.33	26.48	28.67

Table 5.16: Cytotoxicity study of DTX solution, ZOL-DTX solution, DTX loaded PBCA-PEG20 NP and PBCA-PEG-ZOL NP in MCF7 after 72 h using MTT assay. Data presented as Mean \pm SEM, n = 3.

Cell line/ time	Formulation	Conc of DTX (nM)	% Viability			Mean of % viability
MCF7/ 72 h	DTX	0.5	84.31	89.07	84.37	85.92
		2	50.05	64.18	77.56	63.93
		8	30.18	33.03	37.96	33.73
	DTX-ZOL	0.5	82.52	78.37	82.24	81.05
		2	47.63	54.02	76.96	59.54
		8	31.37	27.63	42.90	33.97
	PLGA-PEG20 NP	0.5	57.95	55.22	63.89	59.02
		2	35.93	54.08	51.00	47.00
		8	19.98	26.21	25.22	23.80
	PLGA-PEG- ZOL NP	0.5	41.66	52.68	55.04	49.80
		2	27.31	42.45	45.21	38.32
		8	20.56	22.33	24.35	22.41

Table 5.17: Cytotoxicity study of DTX solution, ZOL-DTX solution, DTX loaded PBCA-PEG20 NP and PBCA-PEG-ZOL NP in BO2 after 48 h using MTT assay. Data presented as Mean \pm SEM, n = 3.

Cell line/ time	Formulation	Conc of DTX (nM)	% Viability			Mean of % viability
BO2/ 48 h	DTX	0.5	99.63	105.41	96.05	100.36
		2	54.71	63.43	60.31	59.48
		8	32.60	44.20	36.91	37.90

	DTX-ZOL	0.5	98.69	107.12	92.91	99.57
		2	57.36	66.37	58.35	60.69
		8	36.88	46.02	38.61	40.50
	PLGA-PEG20 NP	0.5	91.38	91.85	76.97	86.73
		2	54.75	68.74	46.10	56.53
		8	29.91	34.49	26.66	30.36
	PLGA-PEG-ZOL NP	0.5	66.63	65.63	56.72	63.00
		2	38.83	49.68	36.32	41.61
		8	31.91	40.86	24.27	32.34

Table 5.18: Cytotoxicity study of DTX solution, ZOL-DTX solution, DTX loaded PBCA-PEG20 NP and PBCA-PEG-ZOL NP in BO2 after 72 h using MTT assay. Data presented as Mean \pm SEM, n = 3.

Cell line/ time	Formulation	Conc of DTX (nM)	% Viability			Mean of % viability
BO2/ 72 h	DTX	0.5	88.02	87.02	83.87	86.30
		2	36.52	36.52	43.14	38.72
		8	21.66	21.66	24.17	22.50
	DTX-ZOL	0.5	87.83	85.83	83.68	85.78
		2	35.98	35.98	40.47	37.48
		8	20.31	20.31	24.38	21.66
	PLGA- PEG20 NP	0.5	84.30	84.30	84.06	84.22
		2	29.00	29.00	35.54	31.18
		8	10.91	10.91	22.00	14.61
	PLGA- PEG-ZOL NP	0.5	36.93	36.93	45.10	39.65
		2	19.26	19.26	28.44	22.32
		8	14.83	14.83	17.94	15.87

Table 5.20: Cytotoxicity study of DTX solution, ZOL-DTX solution, DTX loaded PBCA-PEG20 NP and PBCA-PEG-ZOL NP in MCF7 and BO2 cell line after 48 h and 72 h using MTT assay.

Condition	DTX	DTX-ZOL	PBCA-PEG20 NP	PBCA-PEG-ZOL NP
MCF7 48 h	6.54	6.84	3.54	2.49
MCF7 72 h	5.23	4.93	2.0	0.46
BO2 48 h	5.78	6.08	4.66	2.18
BO2 72 h	3.39	3.24	2.6	0.36

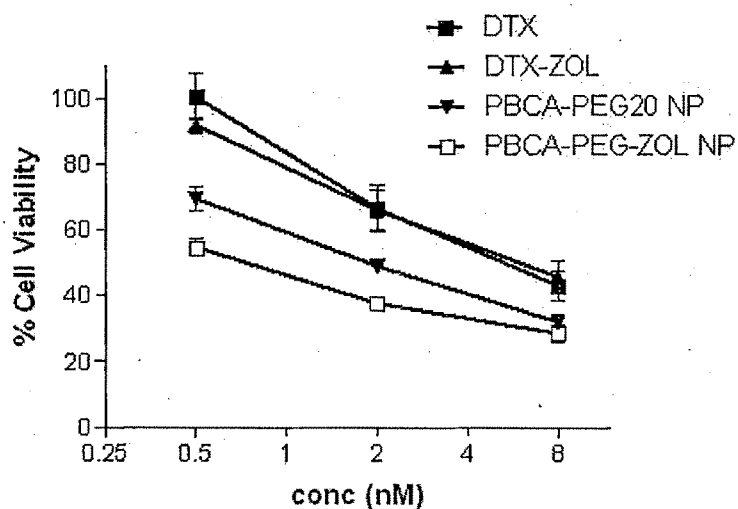


Figure 5.24: Cytotoxicity study of DTX solution, ZOL-DTX solution, DTX loaded PBCA-PEG20 NP and PBCA-PEG-ZOL NP in MCF7 after 48 h using MTT assay. Data presented as Mean \pm SEM, n = 3.

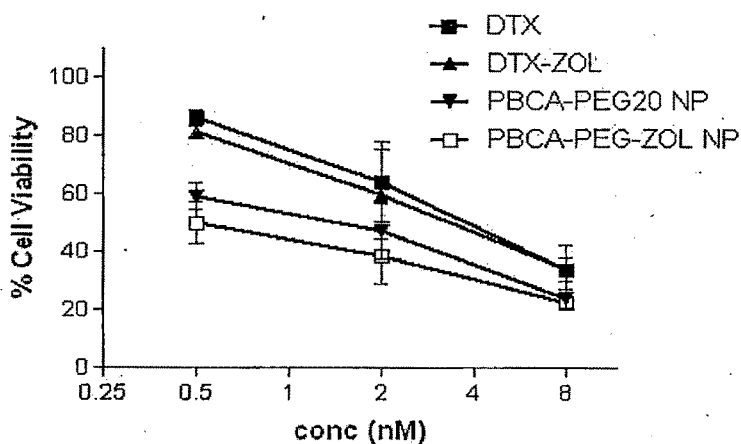


Figure 5.25: Cytotoxicity study of DTX solution, ZOL-DTX solution, DTX loaded PBCA-PEG20 NP and PBCA-PEG-ZOL NP in MCF7 after 72 h using MTT assay. Data presented as Mean \pm SEM, n = 3.

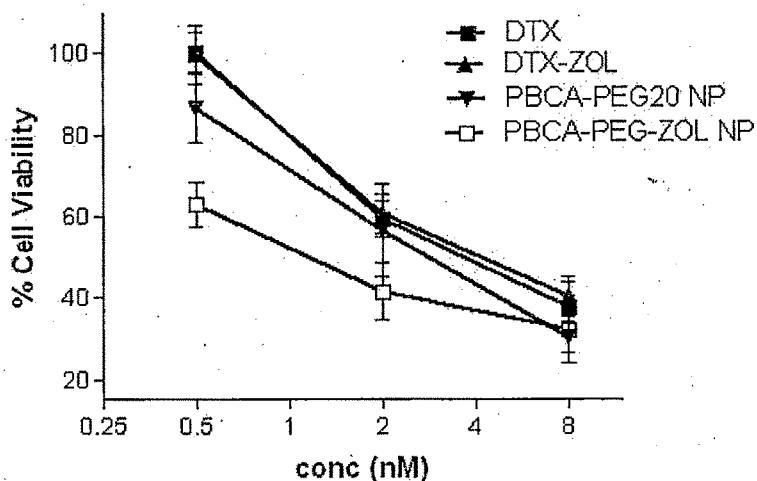


Figure 5.26: Cytotoxicity study of DTX solution, ZOL-DTX solution, DTX loaded PBCA-PEG20 NP and PBCA-PEG-ZOL NP in BO2 after 48 h using MTT assay. Data presented as Mean \pm SEM, n = 3.

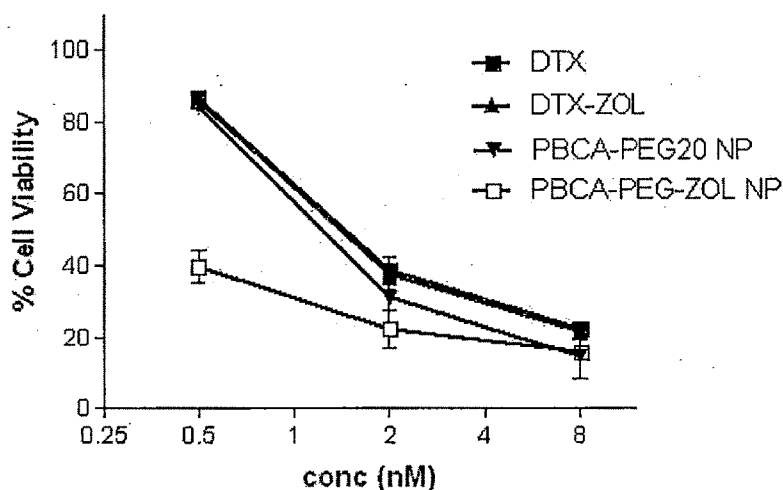


Figure 5.27. Cytotoxicity study of DTX solution, ZOL-DTX solution, DTX loaded PBCA-PEG20 NP and PBCA-PEG-ZOL NP in BO2 after 72 h using MTT assay. Data presented as Mean \pm SEM, n = 3.

5.9 Cell cycle analysis

Analysis of a population of cells' replication state can be achieved by fluorescence labeling of the nuclei of cells in suspension and then analyzing the fluorescence properties of each cell in the population. The distribution of DNA in the cell replication state was studied by flow cytometry (Panyam and Labhasetwar, 2003; Vega et al. 2006). Quiescent and G1 cells will have one copy of DNA and will therefore have 1X fluorescence intensity. Cells in G2/M phase of the cell cycle will have two copies of DNA and accordingly will have 2X intensity. Since the cells in S phase are synthesizing DNA they will have fluorescence values between the 1X and 2X populations (Fig. 5.28). The resulting histogram consists of three populations: two Gaussian curves (1X and 2X peaks) and the S phase population. Adjacent populations overlap each other. Because of this, a modeling program is required to deconvolute the populations and assign percentage values to each population. Expert and subjective review of the modeling software's cell cycle phase percentage assignment is the final stage of cell cycle analysis prior to reporting the results.

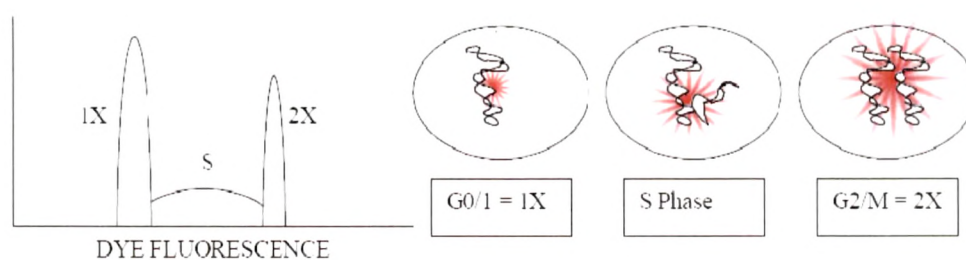


Figure 5.28: Schematic presentation of principle for cell cycle analysis using DNA intercalating fluorescence probe in flow cytometry.

5.9.1 Protocol of cell cycle analysis

1×10^5 cells per well were seeded on 6 well plate and allowed to attach and grow for 24 h. Cells were incubated with 2 ml, 5 nM DTX, DTX loaded PLGA-PEG, PLGA-PEG-ZOL NPs, PBCA-PEG20 NP and PBCA-PEG-ZOL NP in media. After 24 h

media was removed, cells were washed with PBS and treated with 200 μ l of trypsin-EDTA to harvest. Incubation media, washing buffer and trypsin-EDTA treated cell were collected together and centrifuged at 1500 rpm for 5 min. The cell pellet was washed twice with PBS and centrifuged. Cells were resuspended in 0.86 ml cold PBS, vortexed at slow speed and 2 ml absolute ethanol was added drop wise to make final concentration 70% v/v. After 15 min of incubation at 4 $^{\circ}$ C, cells were resuspended in 250 μ l staining PBS solution composed of RNase A (0.1 mg/ml), Propidium iodide (10 μ g/ml) and Triton X 100 (0.05 %) and incubated at room temperature in dark for 20 min. After incubation for 1 h, cell cycle distribution was determined by analyzing 10,000 cells in FACS (Canto-II, BD) and recording signal from Texas red channel. Sections were made in the histogram of count vs. intensity to calculate ratio of cells under Go/G1 (X), S (X+), G2/M phase (2X) and under apoptosis (2X-). Experiment was performed in triplicates.

5.9.2 Cell cycle analysis of PLGA NPs

Analysis of a cell population in each replication state can be achieved by fluorescence labeling of the nuclei with PI staining and then estimating DNA content by FACS analysis. Cell cycle analysis has been performed by FACS using PI staining in BO2 cell line after treatment with DTX, DTX loaded PLGA-PEG20 NP and PLGA-PEG-ZOL NPs. Fig. 9 represent cell cycle distribution of control group having $62.35 \pm 2.64\%$ cells in G0/G1 phase, $12.69 \pm 1.02\%$ in S phase, $22.89 \pm 1.23\%$ cells in G2/M and only $2.07 \pm 0.22\%$ cells in Sub G0/G1 phase (Fig. 5.29). After treatment with DTX the cell cycle arrest has been observed and the majority of cells ($60.74 \pm 2.29\%$) get arrested at G2/M check point with only $6.31 \pm 0.53\%$ cells at Sub G0/G1 phase (Fig. 5.29). Treatment with PLGA-PEG NPs showed similar blockage at G2/M check point as compared to DTX treatment. Almost 1.87 times increase in cell population ($11.84 \pm 0.76\%$) at Sub G0/G1 phase was observed which represent increase in apoptosis (Fig. 5.29). Although, the blockage was remaining stalemate at G2/M check point with PLGA-PEG-ZOL NPs treatment (Fig. 5.29), the PLGA-PEG-ZOL NPs showed significant increase in amount of apoptotic cells at Sub G0/G1 phase (2 times and 4 times as compared to PLGA-PEG NPs and DTX, respectively). Here, results signified effectiveness of PLGA-PEG-ZOL NPs as an effective carrier for DTX among tested formulations. In case of NPs mediated targeted therapy more drug is available at the site of action (following sustained drug release) for a longer period of

time than drug in solution, resulting in greater efficiency of the NP in arresting cell growth. ZOL could facilitate the intracellular delivery of DTX loaded NP, thus better allowing DTX and ZOL for cytotoxic effect and resulting in higher inhibition of cell proliferation.

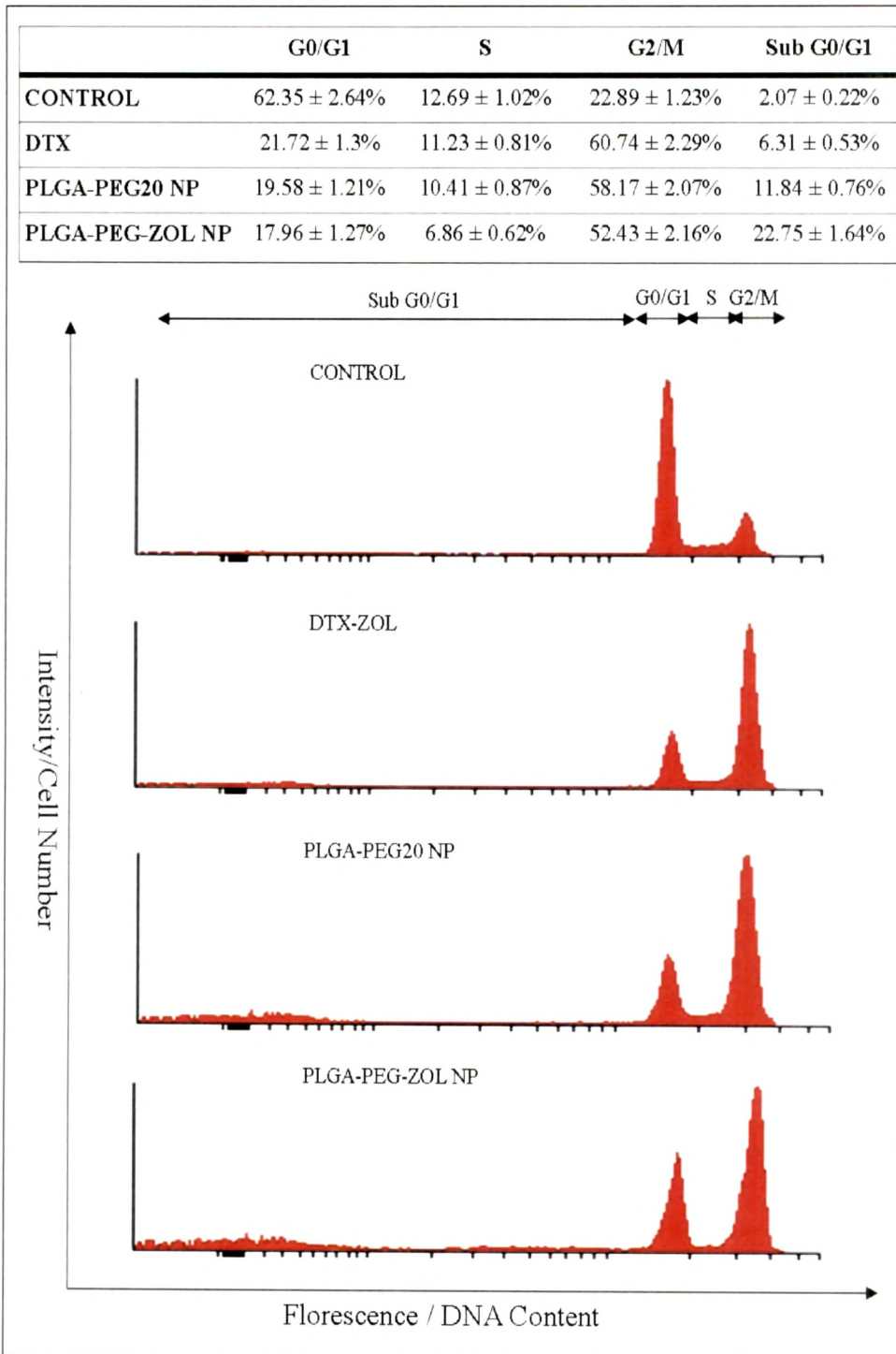


Figure 5.29: Cell cycle analysis in BO2 cell line after treatment of (a) Control (PBS), (b) DTX solution, DTX loaded (c) PLGA-PEG20 NP and (d) PLGA-PEG-ZOL NP by PI staining using FACS technique. Data presented as Mean ± SEM, n = 3.

5.9.3 Cell cycle analysis of PBCA NPs

Analysis of a cell population in each replication state can be achieved by fluorescence labeling of the nuclei with PI staining and then estimating DNA content by FACS analysis (David L. Morse et al 2005). Cell cycle analysis has been performed by FACS using PI staining in BO2 cell line after treatment with DTX, DTX loaded PBCA-PEG and PBCA-PEG-ZOL NPs. Fig. 5.30 represent cell cycle distribution of control group having $62.35 \pm 2.64\%$ cells in G0/G1 phase, $12.69 \pm 1.02\%$ in S phase, $22.89 \pm 1.23\%$ cells in G2/M and only $2.07 \pm 0.22\%$ cells in Sub G0/G1 phase (Figure 5.30). After treatment with DTX the cell cycle arrest can be seen and majority of cell ($60.74 \pm 2.29\%$) get arrested at G2/M check point with only $6.31 \pm 0.53\%$ cells at Sub G0/G1 phase. Treatment with PBCA-PEG NPs showed similar blockage at G2/M check point as compared to DTX treatment, but almost 245% increase ($15.49 \pm 0.86\%$) at Sub G0/G1 phase was observed which represent increase in apoptosis. After treatment with PBCA-PEG-ZOL NPs, blockage at G2/M check point does not change significantly as DTX and PBCA-PEG NPs treatment with significant change in amount of apoptotic cells at Sub G0/G1 phase showing more and more cells underwent apoptotic cell death (2.5 times and 6.2 times as compared to PBCA-PEG NPs and DTX, respectively) which signifies effectiveness of PBCA-PEG-ZOL NPs as an effective carrier for DTX among tested formulations. It can be said that in case of NP mediated targeted therapy more drug is available at the site of action (following sustained drug release) for a longer period of time than drug in solution, resulting in greater efficiency of the NP in arresting cell growth. ZOL could have facilitated the intracellular delivery of DTX loaded NP, thus better allowing DTX and ZOL for cytotoxic effect and resulting in higher inhibition of cell proliferation.

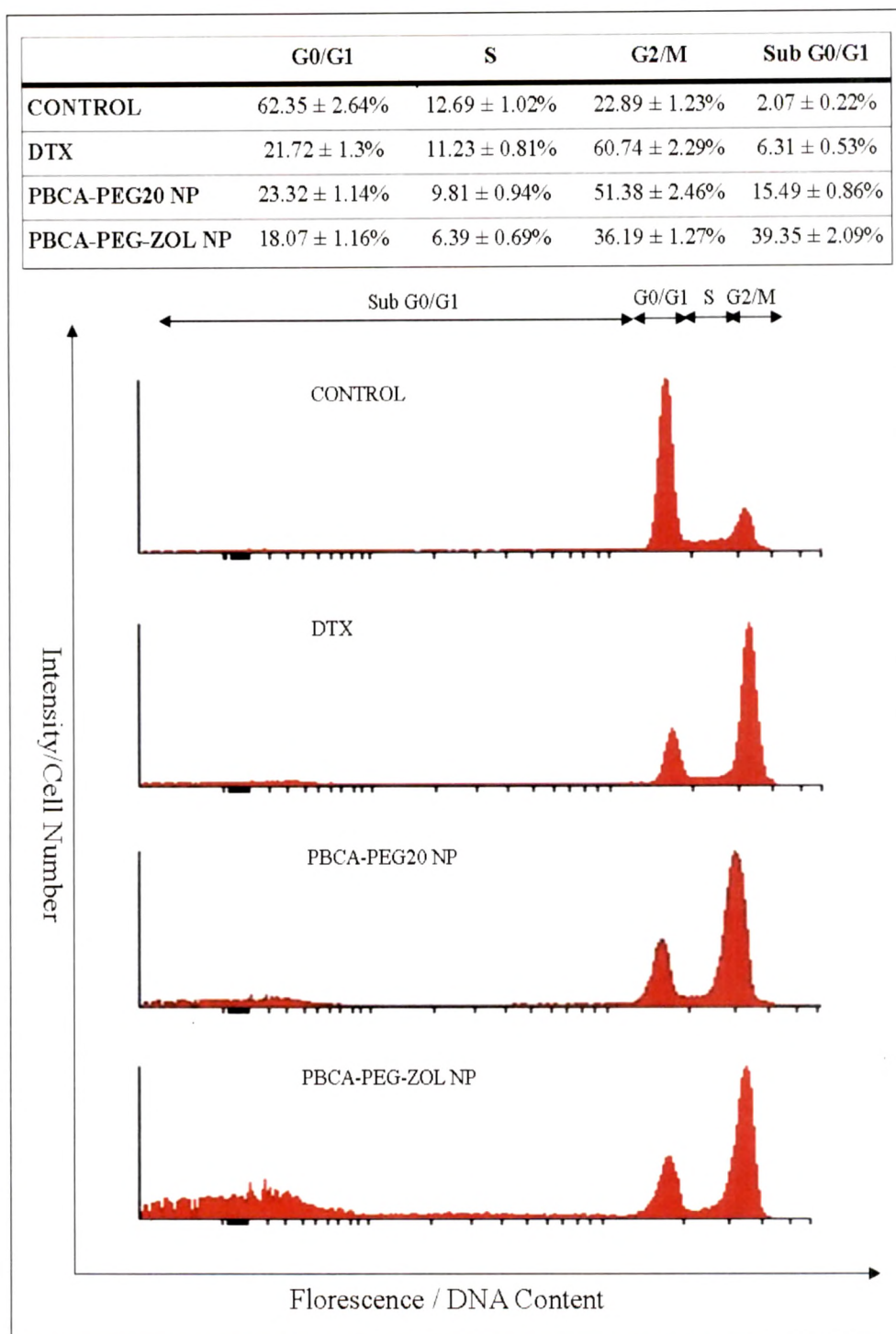


Figure 5.30: Cell cycle analysis in BO2 cell line after treatment of (a) Control (PBS), (b) DTX solution, DTX loaded (c) PBCA-PEG20 NP and (d) PBCA-PEG-ZOL NP by PI staining using FACS technique. Data presented as Mean ± SEM, n = 3.

5.10 Apoptosis using annexin V-FITC and PI marker

Cells undergoing apoptosis show characteristic morphological and biochemical features. The characteristics include chromatin aggregation, nuclear and cytoplasmic condensation, while necrosis displays a direct injury to the cell. Determination of cell death mechanism is important to compare effectiveness of NP formulations. Apoptosis study of prepared NPs was conducted using Annexin V staining procedure in MCF7 and BO2 cell lines. This assay takes advantage of the fact that phosphatidylserine (PS) is translocated from the inner (cytoplasmic) leaflet of the plasma membrane to the outer (cell surface) leaflet soon after the induction of apoptosis. Annexin V protein has a strong, specific affinity for PS which can be used as a probe for estimation (Susin SA et al, 2000).

5.10.1 Protocol for apoptosis study using annexin V-FITC marker

Induction of apoptosis could be studied by flow cytometry using annexin V-FITC as a specific apoptotic marker (Panyam and Labhasetwar, 2003; Vega et al. 2006). 1×10^5 Cells were seeded on 6 well plates and allowed to attach and grow for 24 h. Cells were incubated with 2 ml (1 nM) DTX, DTX loaded PLGA-PEG20 NP, PLGA-PEG-ZOL NPs, PBCA-PEG20 NP and PBCA-PEG-ZOL NP. After 48 h, cells were harvested and washed. 1×10^5 cells were suspended in 100 μ l binding buffer and stained with PI (10 μ l, 1 mg/ml) and Annexin V-FITC (5 μ l), mixed well using vortex shaker and kept for binding. After 30 min, another 200 μ l binding buffer was added and suspension was analyzed using FACS at Texas red and FITC channel (Canto-II, BD). The intensity plot of FITC vs. Texas Red was sectioned in four quarters to differentiate stained and unstained cells. Based on four quarters, percentage of cells in early apoptotic cells (FITC positive and PI negative), late apoptosis (FITC and PI positive), necrotic (FITC negative and PI positive) and live cells (FITC negative and PI negative) were calculated. In fig. 9, upper Left square among four square shows proapoptotic cells, upper right shows late apoptotic cells, lower left show normal cells and lower right shows necrotic cells.

5.10.2 Apoptosis evaluation of PLGA NPs

Cells undergoing apoptosis shows characteristic morphological and biochemical features. The characteristics include chromatin aggregation, nuclear and cytoplasmic condensation, while necrosis displays a direct injury to the cell. Determination of cell

death mechanism is important to compare effectiveness of NP formulations. Apoptosis study of prepared NPs was conducted using Annexin V staining procedure in MCF7 and BO2 cell lines. This assay takes advantage of the fact that phosphatidylserine (PS) is translocated from the inner (cytoplasmic) leaflet of the plasma membrane to the outer (cell surface) leaflet soon after the induction of apoptosis. Annexin V protein has a strong, specific affinity for PS which can be used as a probe for estimation (Susin SA et al, 2000). In MCF7 cells, control treatment group shows negligible presence of apoptosis and necrotic cells (less than 5%) (Fig. 5.31). The percentage of apoptotic cells was higher in case of cells treated with DTX loaded PLGA-PEG-ZOL NPs (32.58%) than with DTX loaded PLGA-PEG NPs (23.03%) or with DTX (14.72%), which is almost 1.4 and 2.2 times (Fig. 5.31). With DTX treatment we observed very few cells (2.14%) at pro-apoptotic phase as compared to DTX loaded PLGA-PEG NPs (3.97%) and DTX loaded PLGA-PEG-ZOL NPs (7.79%). All formulations showed negligible amount of necrotic cells while control group shows negligible apoptotic activity. DTX loaded PLGA-PEG-ZOL NPs were able to cause a significant increase in programmed cell death as 32.58% cells were observed in late apoptotic phase in comparison to 14.72% and 23.03% cell death when treated with DTX and DTX loaded PLGA-PEG NPs.

In apoptosis study with BO2 cell line, similar results were obtained. The increased number of cells at pro-apoptotic and almost negligible number of cells at necrotic phase were observed. We found the majority of cells present at the late apoptotic and early apoptotic phase when treated with DTX, DTX loaded PLGA-PEG and PLGA-PEG-ZOL NPs. Control treatment showed less than 5% cell death, either programmed or un-programmed. In case of MCF 7, DTX loaded PLGA-PEG-ZOL NPs showed 34.39% cells at late apoptosis as compared to DTX solution (7.46%) and DTX loaded PLGA-PEG NPs (22.64%) (Fig. 5.32). The distribution of early apoptotic cells was 6.07%, 12.95% and 13.21% for DTX solution, DTX loaded PLGA-PEG NPs and PLGA-PEG-ZOL NPs, respectively (Fig. 5.32). After internalization, NPs might be activated apoptotic signals at very low dose by reducing threshold required for activation. Targeted delivery had showed enhanced apoptosis by more receptor mediated endocytosis which made more concentration of drug available for action. Sustained cytoplasmic delivery of DTX from NPs coupled with ZOL resulted in more enhanced therapeutic potency of the NPs by apoptosis than unconjugated NPs, thus

supporting the hypothesis that ZOL modified NP can serve as effective delivery vehicles to bone metastasis and cancer.

Table 5.21: Apoptosis estimation in MCF7 and BO2 cell lines after treatment of Control (PBS), DTX solution, DTX loaded PLGA-PEG20 NP and PLGA-PEG-ZOL NP by Annexin V-FITC & PI staining using FACS technique. Data presented as Mean, n = 3.

	Formulation	Live cells	Early Apoptosis	Late Apoptosis	Necrotic cells
MCF7	DTX	95.44	0.42	3.36	0.78
	DTX-ZOL	82.19	2.14	14.72	0.94
	PLGA-PEG20 NP	66.32	10.05	22.13	1.48
	PLGA-PEG-ZOL NP	59.63	7.94	30.96	1.47
BO2	DTX	95.4	0.43	3.36	0.78
	DTX-ZOL	82.19	2.14	14.72	0.94
	PLGA-PEG20 NP	62.97	12.95	22.64	1.44
	PLGA-PEG-ZOL NP	13.21	13.21	34.39	0.39

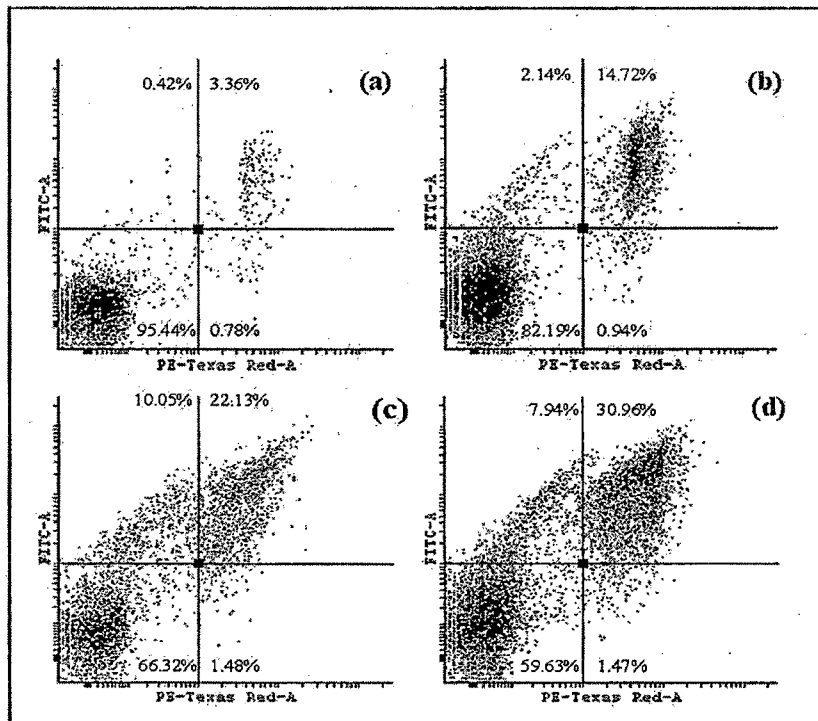


Figure 5.31: Apoptosis estimation in MCF7 cell lines after treatment of Control (PBS), DTX solution, DTX loaded PLGA-PEG20 NP and PLGA-PEG-ZOL NP by Annexin V-FITC & PI staining using FACS technique. Data presented as Mean \pm SEM, n = 3.

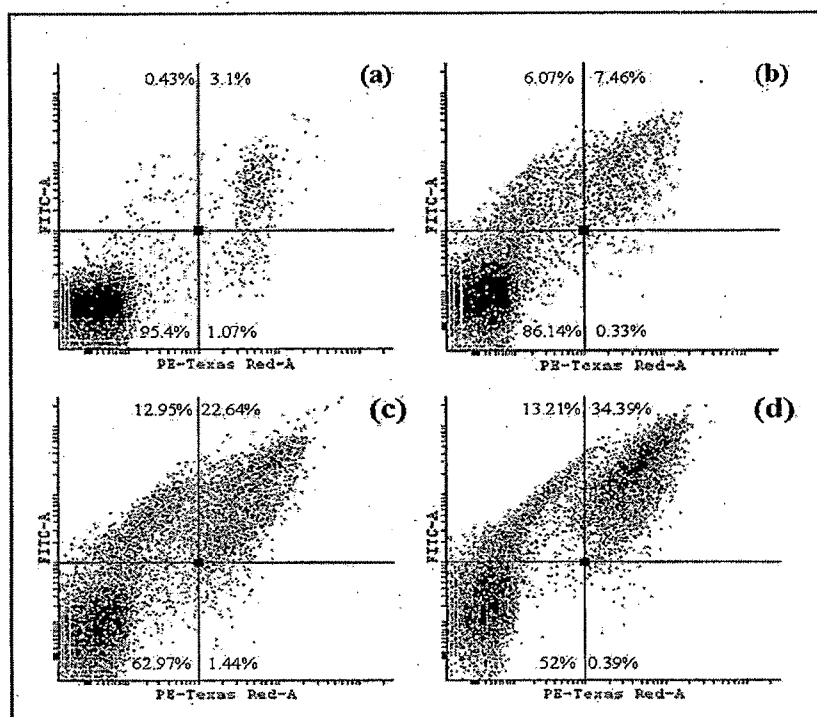


Figure 5.32: Apoptosis estimation in BO2 cell lines after treatment of Control (PBS), DTX solution, DTX loaded PLGA-PEG20 NP and PLGA-PEG-ZOL NP by Annexin V-FITC & PI staining using FACS technique. Data presented as Mean \pm SEM, n = 3.

5.10.3 Apoptosis evaluation of PBCA NPs

In MCF-7 cells, control treatment group shows negligible presence of apoptosis and necrotic cells (less than 4.5%) (Fig. 5.33). The percentage of apoptotic cells was higher in case of cells treated with DTX loaded PBCA-PEG-ZOL NPs (32.58%) than with DTX loaded PLGA-PEG NPs (23.03%) or with DTX (14.72%), which is almost 1.4 and 2.2 times (Fig. 5.33). While DTX had very few cells i.e. 2.14% in pro-apoptotic phase, DTX loaded PLGA-PEG NPs showed almost 2 times pro-apoptotic cells (3.97%) whereas DTX loaded PLGA-PEG-ZOL NPs showed 7.79% cells within

pro-apoptotic phase. All formulations show negligible amount of necrotic cells (< 2%) while control group shows negligible apoptotic activity. Thus, DTX loaded PBCA-PEG-ZOL NPs were able to cause a significant increase in programmed cell death as 32.58% cells were observed in late apoptotic phase in comparison to cells treated with DTX and DTX loaded PLGA-PEG NPs.

In apoptosis studies with BO2 cell line, similar results were obtained with increased pro-apoptotic (from 0.43% in control cells to 13.61% in PBCA-PEG-ZOL NPs treated cells) and almost negligible number of cells in necrotic phase (< 2.6%). We found major presence of late apoptotic and early apoptotic phase when treated with DTX, DTX loaded PBCA-PEG and PBCA-PEG-ZOL NPs. Control treatment again showed less than 5% cell death, either programmed or unprogrammed. On the lines of MCF7 cell line, DTX loaded PBCA-PEG-ZOL NPs showed 36.39% cells with late apoptosis as compared to DTX solution and DTX loaded PBCA-PEG NPs which found only 7.46% and 20.9%, late apoptotic cell death respectively (Fig. 5.34). The distributions of early apoptotic cells were 6.07%, 12.47% and 13.61% for DTX solution and DTX loaded PBCA-PEG NPs and PBCA-PEG-ZOL NPs, respectively (Fig. 5.34). After internalization, NPs might activated apoptotic signals at much reduced dose by dipping threshold require for activation. Targeted delivery had showed enhanced apoptotic activity by more RME which made more drugs available for action. Sustained cytoplasmic delivery of the DTX from NPs coupled with ZOL resulted in more enhanced therapeutic potency of the NPs by apoptosis as compared with unconjugated NPs, thus supporting the hypothesis that ZOL modified NPs can serve as effective delivery vehicles to bone metastasis and cancer.

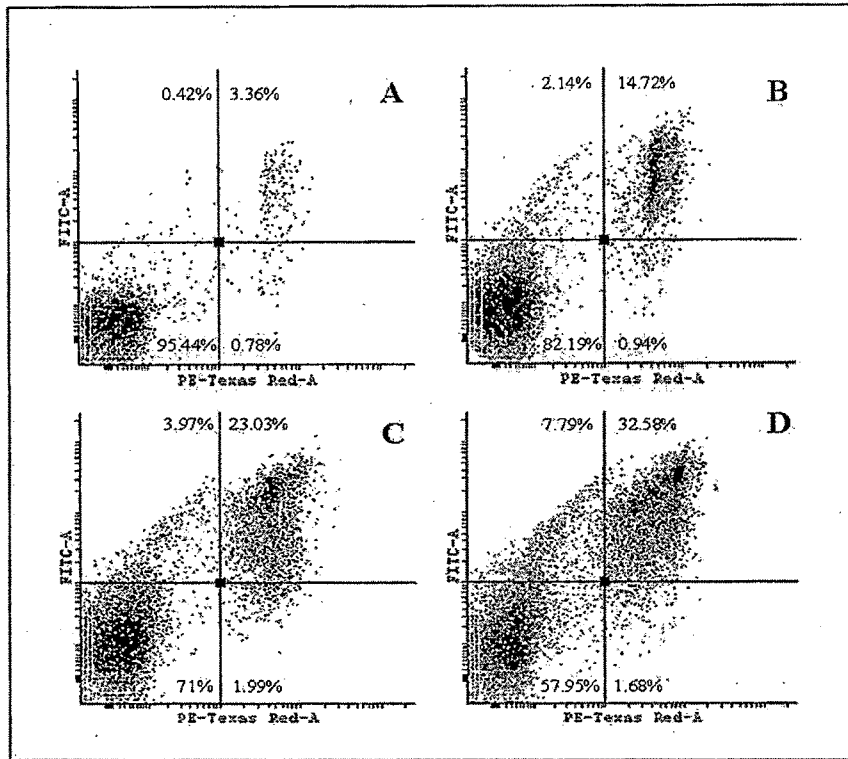


Figure 5.33: Apoptosis estimation in MCF7 cell lines after treatment of Control (PBS), DTX solution, DTX loaded PLGA-PEG20 NP and PLGA-PEG-ZOL NP by Annexin V-FITC & PI staining using FACS technique. Data presented as Mean \pm SEM, n = 3.

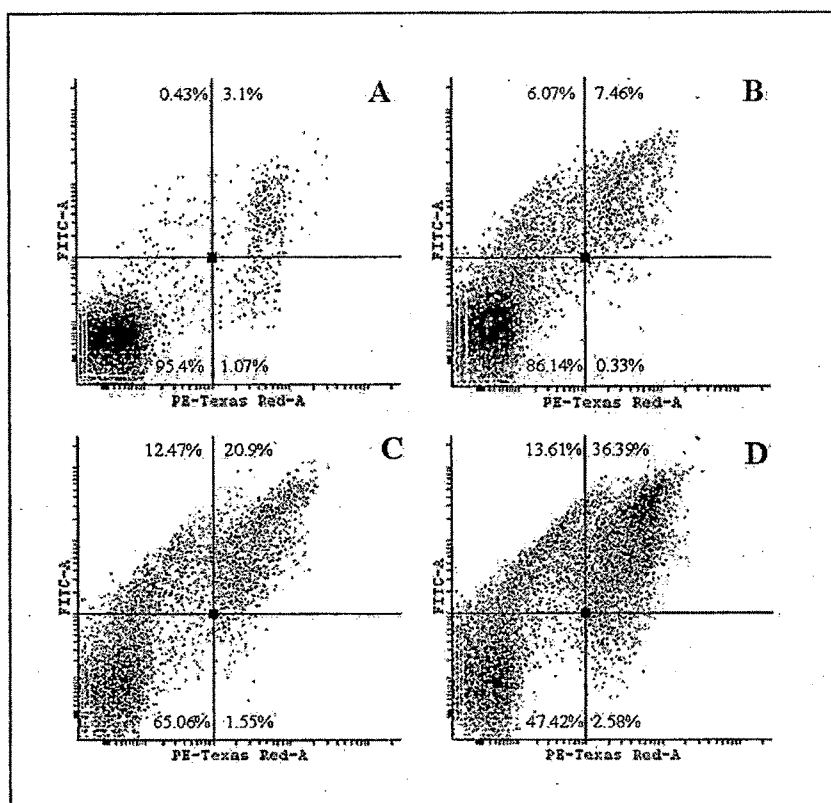


Figure 5.34: Apoptosis estimation in BO2 cell lines after treatment of Control (PBS), DTX solution, DTX loaded PLGA-PEG20 NP and PLGA-PEG-ZOL NP by Annexin V-FITC & PI staining using FACS technique. Data presented as Mean \pm SEM, $n = 3$.

5.11 IPP and ApppI measurement

The intracellular mevalonate pathway (MVP) produces several biomolecules essential for cell function, such as cholesterol, dolichol and respiratory quinines (Goldstein, 1990). The metabolites of the pathway include isoprenoid pyrophosphates consisting of a five-carbon building block termed isoprene unit. The isoprenyl intermediates of the pathway are produced by sequential condensation reaction of isopentenyl pyrophosphate (IPP) and dimethylallyl pyrophosphate (DMAPP) yielding metabolites with carbon chain length of 10, 15 or 20 carbons, corresponding geranyl (GPP), farnesyl (FPP) and geranyl geranyl pyrophosphates (GGPP), respectively (Barkovich and Liao, 2001). The chain elongation reactions are catalyzed by FPP and GGPP synthases. FPP and GGPP are substrates for protein prenyl transferases catalyzing

farnesylation and geranygeranylation reactions of small GTPases signaling proteins, enabling their trafficking to cell membranes (McTaggart, 2006).

MVP is a site of action for nitrogen-containing bisphosphonates (N-BPs), drugs used for treatment of various metabolic bone diseases (Fig. 5.35). These diseases express high bone resorption, mediated by increase in either number or activity of osteoclasts. The anti-resorptive activity of N-BPs is most likely due to their direct effect on mature osteoclasts (Rogers, 2011). Moreover, it is becoming evident that N-BPs also have an anti-tumorial effect *in vitro* and *in vivo* (Monkkonen et al, 2006; Monkkonen et al, 2007). The molecular mechanism of action of the N-BPs (such as zoledronic acid, ZOL) is *via* inhibition of the FPP synthase, the key enzyme of the mevalonate pathway, in particular, due to consequent depletion of prenylated GTPases. However, accumulation of the unprenylated GTPases and subsequent inappropriate activation of downstream signaling pathways may also account for the anti-resorptive effect of N-BPs rather than loss of the prenylated proteins. Based on our recent findings we have proposed an additional mechanism of action for N-BPs. The inhibition of FPP synthase by N-BPs, in addition to depletion of the biosynthesis of FPP and GGPP, leads to accumulation of the early metabolites of mevalonate pathway, IPP. (Jauhiainen et al, 2009).

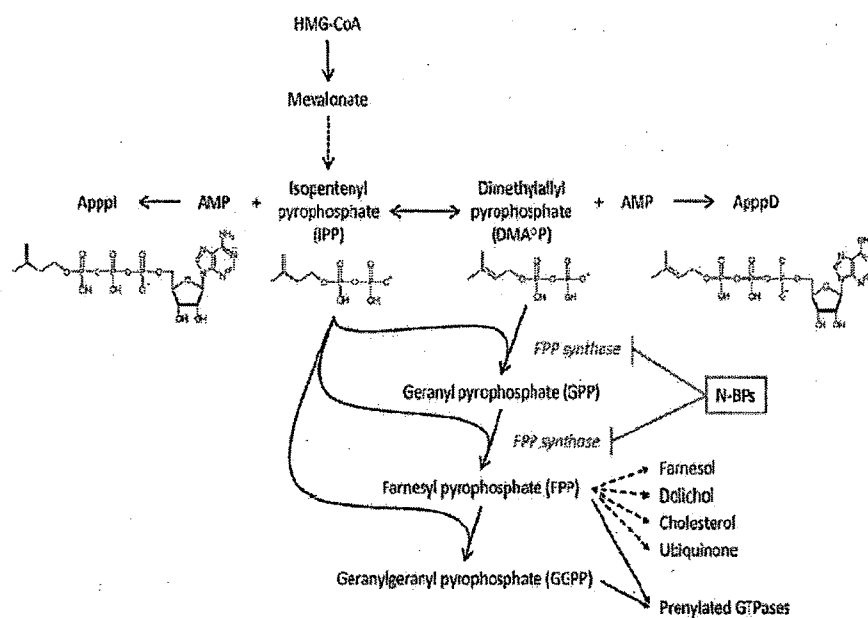


Figure 5.35: Schematic presentation of the mevalonate pathway (MVP) and molecule structures of IPP and ApppI (Jauhiainen et al., 2009)

The amount of these metabolites in excess of their physiological levels induces biosynthesis of a novel ATP analog ApppI (triphosphoric acid 1-adenosin-5'-yl ester 3-(3-methylbut-3-enyl) ester) as a conjugation reaction of IPP to 5'-adenosine monophosphate (AMP), catalyzed presumably by aminoacyl-tRNA-synthetases (Hannu Monkkonen et al, 2006). Our results show that ApppI causes apoptosis by blocking the mitochondrial adenine nucleotide translocase (ANT) and thus can evoke direct apoptosis. We have established the IPP accumulation and subsequent ApppI formation *in vitro* in J774 macrophage like cells after treatment with several N-BPs as well as in different cancer cells after exposure to ZOL. Also, similar effect of ZOL treatment was seen *in vivo* in mouse peritoneal macrophages (Rogers, 2011).

5.11.1 Cells treatment and sample preparation for LC-MS

Sample treatment and preparation was performed as per earlier reported method (Marjo Jauhiainen et al 2009). MCF7 and BO2 cells were seeded in 6 well plates at the density of 4×10^5 cells per well and incubated for 24 h to allow cell attachment. After 24 h, cells were incubated/treated with 1 $\mu\text{g/ml}$, 2 ml of ZOL solution and PLGA-PEG-ZOL NP along with control group (PBS) for 24 h. To extract anylates from cell line samples, cell culture plates was treated with ice cold acetonitrile (300 μL) followed by ice cold milliQ water (200 μL). The adherent cell line was scrapped and performed pipette mixing followed by centrifugation (13,000 \times g, 3 min, 4°C). The supernatant was transferred in another tube and evaporated until complete dryness using vacuum centrifugation and stored at -20°C until LC-MS analysis. Before analysis, the content was dissolved in MilliQ water (150 μL) having 0.25 mM NaF and Na₃VO₄ phosphatase inhibitors and 1.0 μM AppCp as internal standard. The cell lysate precipitate was digested with 1M NaOH at 60°C for 2 h and performed for total protein content estimation using modified Bradford procedure (Bio-Rad, Hercules, CA, USA) using bovine serum albumin as a standard protein on plate counter (Wallac Victor2) at 595 nm. The final concentration of IPP and ApppI was presented as nM per mg of protein.

5.11.2 Estimation of IPP and ApppI using LC-MS

All conditions have been previously described in detail by Monkkonen et al. (2000) and Marjo Jauhiainen et al (2009). On-line HPLC-ESI MS measurements were carried out using an Agilent 6410 Triple Quad LC/MS for the analysis of IPP, ApppI and AppCCI2 (standard). Instrument was equipped with an electrospray ionization source (EIS) and operated on negative ion mode. For the Agilent triple quadrupole instrument optimized parameters were following: drying gas temperature was kept at 300°C, gas flow at 8 mL/min, nebulizer gas pressure operated at 40 psi and capillary voltage was kept at - 4500V. Negative full scan mass spectra were performed in the mass range of m/z 60–650 at above mentioned condition. Parent ion abundance with highest intensity was indentified using fragmentor voltages of 120 V for IPP, and 140V for ApppI and internal standard (ISTD) AppCp. Individual product ion (MS2) spectra were recorded using collision induced dissociation (CID) in the collision cell with nitrogen gas. Most intense product ion signal was achieved when offset voltages kept at 15 eV, 27 eV and 30 eV for detection of IPP, ApppI and internal standard (AppCp) respectively. Following transitions were optimized for multiple reactions monitoring (MRM): m/z 245→79 for IPP, m/z 574→227 for ApppI and m/z 504→157 for internal standard (AppCp). Agilent Mass Hunter Workstation software was used for data acquisition.

5.11.3 Quantification of the total amounts of IPP and ApppI

The analysis method was validated using IPP and ApppI standards. The limit of quantification (LOQ) was estimated as the lowest estimation with the percent relative standard deviation (RSD %) value lower than 20% and signal-to-noise ratio remained greater than 10:1. All calibration samples were prepared freshly on each day of analysis. The calibration area was selected in range from 0.010 μ M to 90.0 μ M for IPP and from 0.030 μ M to 30.0 μ M for ApppI. The calibration curve was obtained in three replicate measurements. Ratio of peak area of analytes and internal standard were plotted against the concentration of the standards.

Treatment with PLGA-PEG-ZOL NPs shown 7.5 times increase in IPP production in comparison to ZOL solution treatment and 61 times higher than control group (Fig. 5.36). ApppI level in MCF-7 cell line after treatment with PLGA-PEG-ZOL NPs was found 6.84 times higher than treatment with ZOL solution (Fig. 5.37). In case of BO2 cell line, IPP production after treatment with PLGA-PEG-ZOL NPs was 3.87 times

higher than ZOL solution and IPP level in control group was below detection level (Fig. 5.38). However, we did not find any ApppI production in BO2 cell line after treatment with PLGA-PEG-ZOL NPs and ZOL solution which was as per our previous experience as BO2 cell line was not shown ApppI up to detectable level. Treatment with DTX was not found to shown production of IPP or ApppI at any concentration. Results evidenced that ZOL in PLGA-PEG-ZOL NPs form significantly enhanced action of ZOL in both cell lines.

Amount of IPP and ApppI were estimated in BO2 and MCF-7 cell lines after treatment with ZOL and PBCA-PEG-ZOL NPs. Fraction of proteins was separated by extraction using acetonitrile:water after cell lysis and estimated using HPLC-ESI-MASS instrument. Results showed that treatment with ZOL solution in MCF-7 cell line found to increase IPP production more than 19 times than control group treated with PBS (Fig. 5.39). Treatment with PBCA-PEG-ZOL NPs showed 7 times increase in IPP production in comparison to ZOL solution treatment and 138 times higher than control group. ApppI level in MCF-7 cell line after treatment with PBCA-PEG-ZOL NPs was found 5.3 times higher than treatment with ZOL solution (Fig. 5.40). In case of BO2 cell line, IPP production after treatment with PBCA-PEG-ZOL NPs was 5.35 times higher than ZOL solution and IPP level in control group was below detection level (Fig. 5.41). However, no ApppI production in BO2 cell line after treatment with PBCA-PEG-ZOL NPs and ZOL solution was found which was as per our previous experience as BO2 cell line did not show production of ApppI up to detectable level (Ref.). Treatment with DTX was not found to shown production of IPP or ApppI at any concentration. Results evidenced that ZOL conjugated to PBCA-PEG NPs can significantly enhanced action of ZOL in both cell lines.

Table 5.22: ApppI accumulation after treatment with ZOL solution and PLGA-PEG-ZOL NP along with control (PBS) in MCF7 cell line.

Sample	ApppI in test sample			Internal Standard	
	RT	Response	Final Conc	RT	Response
Control	6.00	169	BDL	5.62	14583
	6.01	177	BDL	5.62	13874

	5.98	204	BDL	5.61	14018
ZOL	6.00	966	12	5.62	14428
	5.98	1155	15	5.61	14225
	6.01	1141	15	5.62	14126
PLGA	6.00	8261	111	5.61	14213
	6.01	11182	115	5.62	14334
	6.00	10660	141	5.62	14498
PBCA	5.99	27352	372	5.62	14166
	6.00	23418	312	5.62	14419
	6.00	36277	489	5.61	14289

Table 5.23: IPP and ApppI accumulation after treatment with ZOL solution and PLGA-PEG-ZOL NP along with control (PBS) in MCF7 cell line.

Cell line	ATP metabolites	Sample tested	Mean conc	Mean protein content	Conc per mg of protein
MCF7	IPP	Control	11	16.43	0.07
		ZOL solution	72	13.59	0.53
		PLGA-PEG-ZOL NP	688	17.09	4.02
		PBCA-PEG-ZOL NP	1546	17.10	9.04
	ApppI	Control	BDL	16.45	-
		ZOL solution	14	13.51	0.10
		PLGA-PEG-ZOL NP	123	17.10	0.72
BO2	IPP	Control	BDL	15.11	-
		ZOL solution	890	15.24	5.84
		PLGA-PEG-ZOL NP	3379	14.89	22.69
		PBCA-PEG-ZOL NP	4683	14.86	31.44

Table 5.24: IPP and ApppI accumulation after treatment with ZOL solution and PLGA-PEG-ZOL NP along with control (PBS). IPP and ApppI in MCF7 cell line and IPP in BO2 cell line.

Sample	IPP in test sample			Internal Standard	
	RT	Response	Final Conc	Response	RT
Control	5.39	467	10	5.62	14583
	5.36	426	9	5.62	13874
	5.39	512	13	5.61	14018
ZOL	5.98	1398	60	5.62	14428
	5.96	1737	79	5.61	14225
	5.98	1699	78	5.62	14126
PLGA	5.97	11088	584	5.61	14213
	5.97	12750	705	5.62	14634
	5.97	14906	774	5.62	14498
PBCA	5.97	28332	1520	5.62	14166
	5.97	25318	1333	5.62	14419
	5.96	33523	1786	5.61	14289

Table 5.25: IPP accumulation after treatment with ZOL solution and PLGA-PEG-ZOL NP along with control (PBS) in BO2 cell line.

Sample	IPP in test sample			Internal Standard	
	RT	Response	Final Conc	RT	Response
Control	6.06	105	BDL	5.55	12942
	6.03	209	BDL	5.63	12585
	6.02	159	BDL	5.63	12588
ZOL	6.00	16854	883	5.63	12966
	6.00	17755	925	5.63	13047
	5.99	17176	863	5.62	13516
PLGA	7.46	45842	3014	7.05	15678
	6.01	65582	3503	5.62	12953

	5.99	66912	3621	5.62	12786
PBCA	5.98	6567	5270	5.63	15679
	5.98	86313	5229	5.61	11444
	5.98	63183	3550	5.61	12314

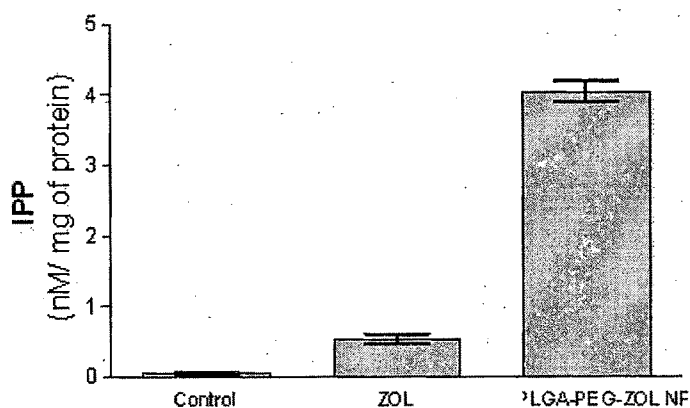


Figure 5.36: IPP accumulation after treatment with ZOL solution and PLGA-PEG-ZOL NP along with control (PBS) in MCF7 cell line.

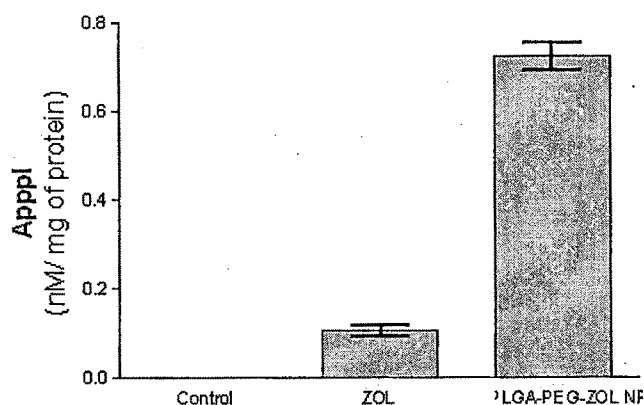


Figure 5.37: AppI accumulation after treatment with ZOL solution and PLGA-PEG-ZOL NP along with control (PBS) in MCF7 cell line.

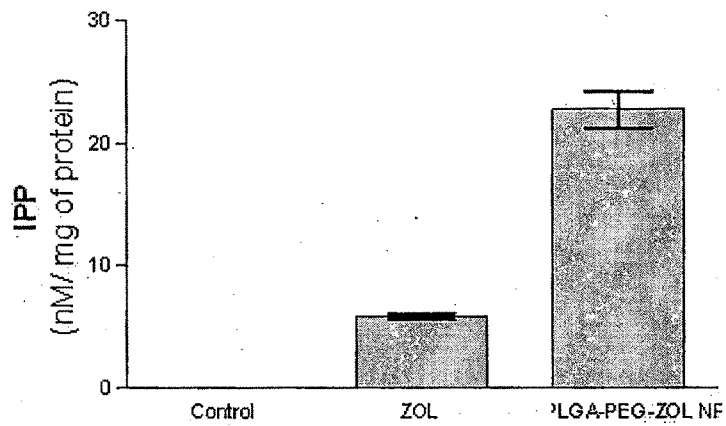


Figure 5.38: IPP accumulation after treatment with ZOL solution and PLGA-PEG-ZOL NP along with control (PBS) in BO2 cell line.

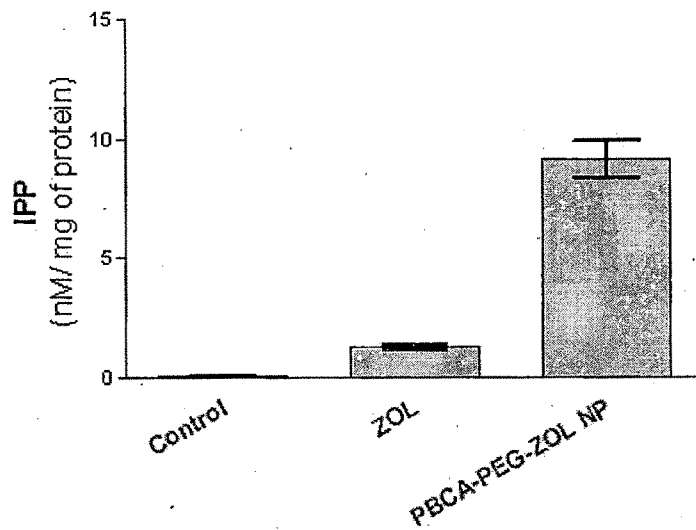


Figure 5.39: IPP accumulation after treatment with ZOL solution and PBCA-PEG-ZOL NP along with control (PBS) in MCF7 cell line.

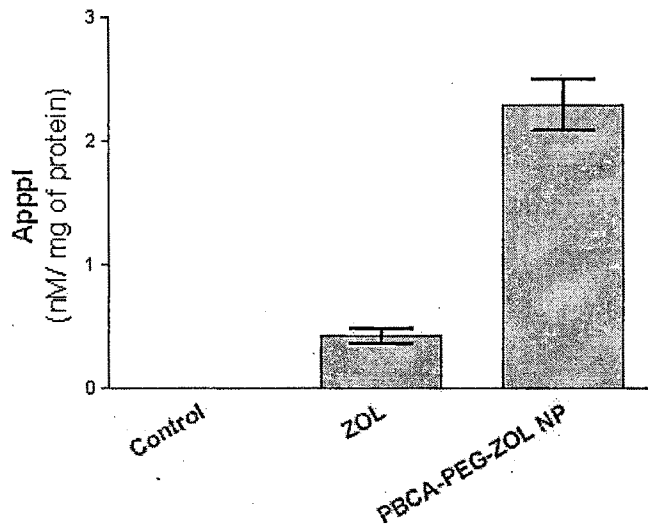


Figure 5.40: Apppl accumulation after treatment with ZOL solution and PBCA-PEG-ZOL NP along with control (PBS) in MCF7 cell line.

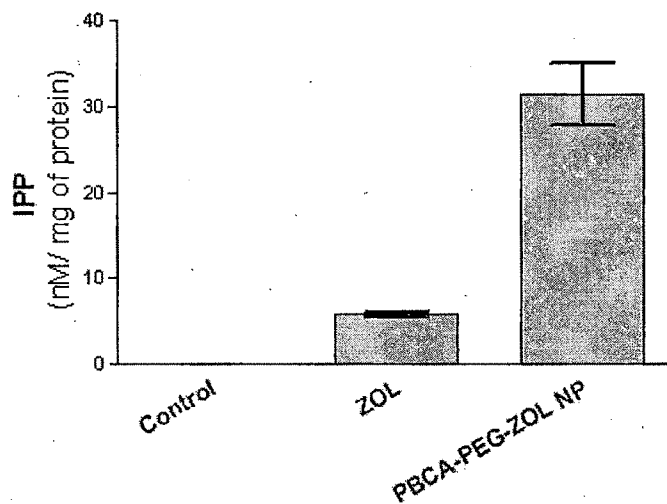


Figure 5.41: IPP accumulation after treatment with ZOL solution and PBCA-PEG-ZOL NP along with control (PBS) in BO2 cell line.

5.12 Conclusion

ZOL anchored, PEGylated and DTX entrapped PBCA and PLGA NP have display potential characteristic as delivery system. *In vitro* phagocytic studies also confirmed effectiveness of PEG coating in repelling phagocytic process. Various *in vitro* cell line study demonstrated

effectiveness of this carrier as a nanocarrier for drug delivery. *In vitro* cell line studies such as cytotoxicity, apoptosis and cell cycle analysis shows enhanced activity with ZOL anchored NPs in comparison to other formulations tested. NPs uptake, uptake route characterization, NPs retention and confocal microscopy revealed change in uptake route of NPs in presence of ZOL. BO2 cell line, having morphology similar to bone metastasis found more prone to ZOL anchored NPs than MCF-7 cell line. ZOL was found to block mevalonate pathway which was a characteristic mechanism of bisphosphonate group. ZOL anchored PLGA NPs and PBCA NPs showed significant increase in retention of apoptotic byproducts such as ApppI and IPP than ZOL alone.

5.13 Reference

1. O. Peyruchaud, B. Winding, I. Pecheur, C.M. Serre, P. Delmas, P. Clezardin, Early detection of bone metastases in a murine model using fluorescent human breast cancer cells: application to the use of the bisphosphonate zoledronic acid in the treatment of osteolytic lesions, *J. Bone Miner. Res.* 16 (11) (2001) 2027–2034.
2. Illum, L., Hunneyball, I.M., Davis, S.S., 1986. The effect of hydrophilic coatings on the uptake of colloidal particles by the liver and by peritoneal macrophages. *Int. J. Pharm.* 29, 53–65.
3. Peracchia, M.T., Fattal, E., Desmaele, D., Besnard, M., Noel, J.P., Gomis, J.M., Appel, M., d'Angelo, J., Couvreur, P., 1999a. Stealth PEGylated polycyanoacrylate nanoparticles for intravenous administration and splenic targeting. *J. Control. Release* 60, 121–128.
4. Gref, R., Minamitake, Y., Peracchia, M.T., Trubetskoy, V., Torchilin, V., Langer, R., 1994. Biodegradable long-circulating polymeric nanospheres. *Science* 263, 1600–1603.
5. Peracchia, M.T., Harnisch, S., Pinto-Alphandary, H., Gulik, A., Dedieu, J.C., Desmaele, D., d'Angelo, J., Muller, R.H., Couvreur, P., 1999b. Visualization of in vitro protein-rejecting properties of PEGylated stealth (R) polycyanoacrylate nanoparticles. *Biomaterials* 20, 1269–1275.
6. Liu LX, Song CN, Song LP, Zhang HL, Dong X, Leng XG. Effects of alkylated-chitosan–DNA nanoparticles on the function of macrophages. *J. Mater. Sci.: Mater. Med.* 2009;20(4):943–948.
7. Mosqueira VCF, Legrand P, Gref R, Heurtault B, Appel M, Barratt G. Interactions between a macrophage cell line (J774A1) and surface-modified poly (D, L-lactide) nanocapsules bearing poly(ethylene glycol). *J. Drug Targeting.* 1999;7(1):65–78.
8. Gref R, Domb A, Quellec P, Blunk T, Müller RH, Verbavatz JM, Langer R. The controlled intravenous delivery of drugs using PEG-coated sterically stabilized nanospheres. *Adv. Drug Delivery Rev.* 1995;16(2-3):215-233.
9. Gref R, Quellec P, Marchand M, Dellacherie E, Lück M, Harnisch S, Blunk T, Müller RH, „Stealth“ corona-core nanoparticles surface modified by polyethylene glycol (PEG): influences of the corona (PEG chain length and surface density) and of the core composition on phagocytic uptake and plasma protein adsorption. *Colloids Surf., B.* 2000;18(3-4),301-313.

10. Peracchia MT, Vauthier C, Passirani C, Couvreur P, Labarre D. Complement consumption by poly(ethylene glycol) in different conformations chemically coupled to poly(isobutyl 2-cyanoacrylate) nanoparticles. *Life Sci.* 1997(b);61(7):749-761.
11. R. Castino, M. Demoz, C. Isidoro, Destination 'lysosome': a target organelle for tumour cell killing? *J. Mol. Recognit.* 16 (2003) 337–348.
12. W.S. Sly, C. Vogler, Brain-directed gene therapy for lysosomal storage disease: going well beyond the blood–brain barrier, *Proc. Natl. Acad. Sci. U. S. A.* 99 (2002) 5760–5762.
13. Lisa M. Bareford, Peter W. Swaan; Endocytic mechanisms for targeted drug delivery; *Advanced Drug Delivery Reviews* 59 (2007) 748–758
14. L. Prasmickaite, A. Hogset, P.K. Selbo, B.O. Engesaeter, M. Hellum, K. Berg, Photochemical disruption of endocytic vesicles before delivery of drugs: a new strategy for cancer therapy, *Br. J. Cancer* 86 (2002) 652–657.
15. E.A. Biessen, H. Vietsch, E.T. Rump, K. Fluiter, J. Kuiper, M.K. Bijsterbosch, T.J. van Berkel, Targeted delivery of oligodeoxynucleotides to parenchymal liver cells in vivo, *Biochem. J.* 340 (Pt 3) (1999) 783–792.
16. C.Mamot,D.C.Drummond,U.Greiser,K.Hong, D.B.Kirpotin, J.D.Marks, J.W. Park, Epidermal growth factor receptor (EGFR)-targeted immunoliposomes mediate specific and efficient drug delivery to EGFR- and EGFRvIIIoverexpressing tumor cells, *Cancer Res.* 63 (2003) 3154–3161.
17. A. Biragyn, P.A. Ruffini, M. Coscia, L.K. Harvey, S.S. Neelapu, S. Baskar, J.M. Wang, L.W. Kwak, Chemokine receptor-mediated delivery directs self-tumor antigen efficiently into the class II processing pathway in vitro and induces protective immunity in vivo, *Blood* 104 (2004) 1961–1969.
18. A.L. Dunehoo,M. Anderson, S.Majumdar, N. Kobayashi, C. Berkland, T.J. Siahaan, Cell adhesion molecules for targeted drug delivery, *J. Pharm. Sci.* 95 (2006) 1856–1872.
19. S. Muro, E.H. Schuchman, V.R. Muzykántov, Lysosomal enzyme delivery by ICAM-1-targeted nanocarriers bypassing glycosylation- and clathrindependent endocytosis, *Molec. Ther.* 13 (2006) 135–141.
20. S. Muro, C. Gajewski, M. Koval, V.R. Muzykántov, ICAM-1 recycling in endothelial cells: a novel pathway for sustained intracellular delivery and prolonged effects of drugs, *Blood* 105 (2005) 650–658.

21. A. Mitra, A. Nan, H. Ghandehari, E. McNeill, J. Mulholland, B.R. Line, Technetium-99m-labeled N-(2-hydroxypropyl) methacrylamide copolymers: synthesis, characterization, and in vivo biodistribution, *Pharm. Res.* 21 (2004) 1153–1159.
22. S. Persiani, W.C. Shen, Increase of poly(L-lysine) uptake but not fluid phase endocytosis in neuraminidase pretreated Madin-Darby canine kidney (MDCK) cells, *Life Sci.* 45 (1989) 2605–2610.
23. T. Fujita, M. Nishikawa, C. Tamaki, Y. Takakura, M. Hashida, H. Sezaki, Targeted delivery of human recombinant superoxide dismutase by chemical modification with mono- and polysaccharide derivatives, *J. Pharmacol. Exp. Ther.* 263 (1992) 971–978.
24. W.J. Chang, K.G. Rothberg, B.A. Kamen, R.G. Anderson, Lowering the cholesterol content of MA104 cells inhibits receptor-mediated transport of folate, *J. Cell Biol.* 118 (1992) 63–69.
25. J.E. Schnitzer, Caveolae: from basic trafficking mechanisms to targeting transcytosis for tissue-specific drug and gene delivery in vivo, *Adv. Drug Deliv. Rev.* 49 (2001) 265–280.
26. N. Murthy, J. Campbell, N. Fausto, A.S. Hoffman, P.S. Stayton, Design and synthesis of pH-responsive polymeric carriers that target uptake and enhance the intracellular delivery of oligonucleotides, *J. Control. Release* 89 (2003) 365–374.
27. G. Batori, L. Cervenak, I. Karadi, Caveolae—an alternative endocytotic pathway for targeted drug delivery, *Crit. Rev. Ther. Drug Carr. Syst.* 21 (2004) 67–95.
28. A. Catizone, A.L. Medolago Albani, F. Reola, T. Alescio, A quantitative assessment of non specific pinocytosis by human endothelial cells surviving in vitro, *Cell. Mol. Biol.* 39 (2) (1993) 155–169.
29. A. Rupper, J. Cardelli, Regulation of phagocytosis and endophagosomal trafficking pathways in *Dictyostelium discoideum*, *Biochim. Biophys. Acta.* 1525 (3) (2001) 205–216.
30. B.D. Chithrani, W.C.W. Chan, Elucidating the mechanism of cellular uptake and removal of protein-coated gold nanoparticles of different sizes and shapes, *Nano Lett.* 7 (6) (2007) 1542–1550.
31. J. Panyam, V. Labhsetwar, Dynamics of endocytosis and exocytosis of poly(D,L-Lactide-co-Glycolide) nanoparticles in vascular smooth muscle cells, *Pharm. Res.* 20 (2) (2003) 212–220.
32. T. Mosmann, Rapid colorimetric assay for cellular growth and survival: application to proliferation and cytotoxicity assays, *J. Immunol. Methods.* 65 (1–2) (1983) 55–63.

33. Sieuwerts AM, Klijn JG, Peters HA, Foekens JA: The MTT tetrazolium salt assay scrutinized: how to use this assay reliably to measure metabolic activity of cell cultures in vitro for the assessment of growth characteristics, IC50- values and cell survival. *Eur J Clin Chem Clin Biochem* 1995;33:813-823.
34. Loveland BE, Johns TG, Mackay IR, Vaillant F, Wang ZX, Hertzog PJ: Validation of the MTT dye assay for enumeration of cells in proliferative and antiproliferative assays. *Biochem Int* 1992;27:501-510.
35. S. Acharya, F. Dilnawaz, S.K. Sahoo. Targeted epidermal growth factor receptor nanoparticle bioconjugates for breast cancer therapy, *Biomaterials*. 30 (29) (2009) 5737–5750.
36. F. Vega, L.J. Medeiros, V. Leventaki, C. Atwell, J.H. Cho-Vega, L. Tian, F.X. Claret, G.Z. Rassidakis, Activation of mammalian target of rapamycin signaling pathway contributes to tumor cell survival in anaplastic lymphoma kinase-positive anaplastic large cell lymphoma. *Cancer Res*. 66 (13) (2006) 6589–6597.
37. S.A. Susin, E. Daugas, L. Ravagnan, K. Samejima, N. Zamzami, M. Loeffler, P. Costantini, K.F. Ferri, T. Irinopoulou, M.C. Prevost, G. Brothers, T.W. Mak, J. Penninger, W.C. Earnshaw, G. Kroemer, Two Distinct Pathways Leading to Nuclear Apoptosis, *J. Exp. Med*. 192 (4) (2000) 571–580.
38. M.J. Rogers, J.C. Crockett, F.P. Coxon, J. Mönkkönen, Biochemical and molecular mechanisms of action of bisphosphonates, *Bone*. doi:10.1016/j.bone.2010.11.008
39. H. Monkkonen, S. Auriola, P. Lehenkari, M. Kellinsalmi, I.E. Hassinen, J. Vepsäläinen, J. Monkkonen, A new endogenous ATP analog (Apppl) inhibits the mitochondrial adenine nucleotide translocase (ANT) and is responsible for the apoptosis induced by nitrogen-containing bisphosphonates, *Br. J. Pharmacol*. 147 (4) (2006) 437–445.
40. M. Jauhainen, H. Mönkkönen, J. Rääkkönen, J. Mönkkönen, S. Auriola, Analysis of endogenous ATP analogs and mevalonate pathway metabolites in cancer cell cultures using liquid chromatography–electrospray ionization mass spectrometry, *J. Chromatogr., B: Anal. Technol. Biomed. Life Sci*. 877 (27) (2009) 2967–2975.